Research Square

Preprints are preliminary reports that have not undergone peer review.
They should not be considered conclusive, used to inform clinical practice,
or referenced by the media as validated information.

A Dual-Stream Deep Learning Model for Full-Cycle Landslide Prediction and Intelligent Risk-Informed Decision-Making

Fengyi Guo
Huazhong University of Science and Technology
Jun Sun
Huazhong University of Science and Technology
Kaixin Huang
Huazhong University of Science and Technology
Bing Lu
China State Construction International Investments Limited
Xin Wang
CSCECwangxin@163.com

China State Construction International Investments Limited

Research Article

Keywords: Landslide prediction, Dual-stream deep learning, Digital twin, Multi-timescale forecasting, Engineering early warning, Intelligent decision scheduling

Posted Date: July 10th, 2026

DOI: https://doi.org/10.21203/rs.3.rs-10156845/v1

License: This work is licensed under a Creative Commons Attribution 4.0 International License.
Read Full License

A Dual-Stream Deep Learning Model for Full-Cycle Landslide Prediction and Intelligent Risk-Informed Decision-Making

Fengyi Guo[1], Jun Sun[2], Kaixin Huang[3], Bing Lu[4], Xin Wang[5]

[1] Doctoral student, Department of Civil and Hydraulic Engineering, Huazhong University of Science and Technology, Wuhan 430074, China,86-18907273058; email: guofengyi@hust.edu.cn

[2] Professor, Department of Civil and Hydraulic Engineering, Huazhong University of Science and Technology, Wuhan 430074, China,86-13886106996; email: sunjunym@hust.edu.cn.

[3] Master student, Department of Civil and Hydraulic Engineering, Huazhong University of Science and Technology, Wuhan 430074, China,86-13870706820; email: huangkx713@hust.edu.cn

[4]Senior engineer, China State Construction International Investments (Hubei) Limited, 430014, Wuhan, Hubei, China Email: lubing@cohl.com

[5]Senior engineer, China State Construction International Investments (Hubei) Limited, 430014, Wuhan, Hubei, China Email: cscecwangxin@163.com (Corresponding author)

Abstract:

Landslide hazard mitigation faces dual demands from short-term emergency response and medium- to long-term engineering planning. Short-term forecasting is essential for immediate actions such as personnel evacuation and equipment deployment, whereas medium- and long-term forecasting guides engineering scheduling, resource allocation, and rainy-season hazard control. Existing data-driven models predominantly focus on short-term displacement

prediction and often lack physical constraints and engineering applicability, making them insufficient for multi-scale and full-cycle disaster-prevention requirements.This study proposes a dual-stream deep learning model that integrates temporal dynamics and physical mechanisms, and further embeds it into a digital-twin platform to enable multi-timescale landslide prediction, risk-indicator assessment, and closed-loop engineering decision-making. The model employs two cooperative branches to capture short-term fluctuations and long-term deformation trends simultaneously, while a co-attention mechanism fuses their complementary information. Based on predicted displacement, we design a set of multi-timescale engineering risk indicators—including a short-term acceleration-sensitivity index, a medium-term trend-risk index, and a long-term integrated deformation index—to systematically map model outputs to four engineering early-warning levels.Within the digital-twin platform, the predictive outputs and risk indicators are visualized to trigger short-term emergency responses, monthly engineering scheduling, and quarterly mitigation planning. The proposed framework is validated using a case study of a rainfall-induced landslide in Yunxi County, Shiyan City, Hubei Province. Results demonstrate that the model reliably captures anomalous displacement patterns across different time horizons, enabling earlier warning issuance, optimized resource deployment, improved personnel and equipment safety, and enhanced engineering-intervention effectiveness.

Keywords

Landslide prediction; Dual-stream deep learning; Digital twin; Multi-timescale forecasting; Engineering early warning; Intelligent decision scheduling

1. Introduction

Landslide hazard mitigation entails dual engineering objectives: short-term emergency response and medium- to long-term stabilization and management. On the one hand, short-term (daily to weekly) forecasting is directly linked to emergency actions such as field personnel evacuation and equipment mobilization. On the other hand, medium- and long-term (monthly to seasonal) trend assessments provide essential foresight for engineering scheduling, financial planning, and resource allocation. However, current monitoring and early-warning systems suffer from significant limitations in engineering practice. Short-term acceleration phases are often detected too late to support timely 24–48 h advanced response. Meanwhile, trend drift in medium- to long-term predictions frequently leads to false alarms or missed alarms, especially during the rainy season, resulting in reduced trust from local communities and engineering units. These deficiencies may further trigger suboptimal emergency funding decisions and improper allocation of engineering resources. Consequently, there is an urgent need within engineering departments for a unified forecasting system capable of maintaining stable performance across short-term, monthly, and quarterly timescales to support reliable multi-horizon decision-making.

In recent years, deep learning approaches—such as LSTM/GRU, Temporal Convolutional Networks (TCN), and Transformers—have demonstrated substantial advantages in short-term displacement forecasting and rolling updates[1–3]. Meanwhile, signal decomposition techniques such as EEMD, CEEMDAN, and VMD effectively mitigate the influence of nonstationary disturbances on prediction performance[4–6]. Nevertheless, most of these methods rely solely on displacement time series and lack explicit physical constraints, limiting their generalization across time periods and across sites [7,8]. Under complex geological

conditions, purely data-driven black-box models are insufficient to support the full-cycle requirements of landslide mitigation—from short-term early warning to medium- and long-term engineering management.

To enhance both model robustness and engineering interpretability, two complementary research directions are emerging in geotechnical and geological engineering. The first focuses on multi-component and multi-scale sequence modeling, in which displacement signals are decomposed into trend, periodic, and stochastic components, followed by feature fusion to better accommodate nonstationarity and seasonality[6,9] . The second embeds physical knowledge—such as mechanical constraints, boundary conditions, and prior relationships—into loss functions or network architectures to mitigate extrapolation biases and improve predictive reliability[10]. However, existing studies often delve deeply into only one of these aspects, and few have realized a unified framework that jointly models temporal data, physical variables, and governing constraints. In particular, comprehensive optimization across multiple timescales and the control of cross-scale error propagation remain largely unexplored[11]。

In view of the above engineering and academic problems, this paper proposes a full-cycle landslide prediction and intelligent risk decision-making framework based on time series + physical dual-flow deep learning (Fig. 1). At the data-processing level, Ensemble Empirical Mode Decomposition (EEMD) is applied to denoise raw monitoring sequences and separate intrinsic components, thereby reducing nonstationary interference. At the model level, a temporal stream built upon TCN and BiLSTM captures short-term displacement dynamics and rainfall-induced fluctuations[12], while a physical stream based on XGBoost learns the influence of physical indicators—acceleration, velocity, and the improved tangential angle—

on medium- to long-term deformation trends[13–15] . At the fusion level, a co-attention mechanism establishes dynamic interactions between the two streams, enabling joint optimization of short-term anomalies and long-term gradual evolution within a unified representation space[16]. Based on predicted displacement, a multi-timescale engineering risk–indicator system is developed. The short-term acceleration-sensitivity index ($\boldsymbol{I_{acc}}$) supports 24-hour advanced warning during the rainy season; the medium-term trend-risk index ($\boldsymbol{I_{trend}}$) guides 30-day engineering scheduling; and the long-term seasonal deformation index ($\boldsymbol{I_{season}}$) assists in quarterly risk zoning and resource allocation. Together with model outputs, these indicators are integrated into a digital-twin platform to achieve closed-loop management of short-term emergency response, monthly engineering scheduling, and quarterly mitigation planning[17]. Validation using a rainfall-induced landslide in Yunxi County, Shiyan, Hubei Province demonstrates that the system accurately identifies short-term acceleration phases, optimizes medium-term resource deployment, and informs seasonal mitigation decisions, thereby significantly improving personnel and equipment safety as well as engineering intervention effectiveness.

The main contributions of this work are as follows:① We develop a dual-stream cooperative prediction model tailored for full-cycle landslide management, enabling displacement forecasting across short-term, monthly, and quarterly timescales.② We embed physical information and a co-attention mechanism within the predictive pipeline, alleviating the extrapolation vulnerability of purely time-series–driven models under complex geological conditions.③ We design a multi-timescale engineering risk–indicator system based on predicted displacement and integrate it with a digital-twin scheduling platform, achieving 24-

hour early warning during rainy seasons, optimized 30-day engineering planning, and quarterly resource allocation. This provides a scalable pathway for intelligent landslide early warning and multi-horizon engineering decision-making.

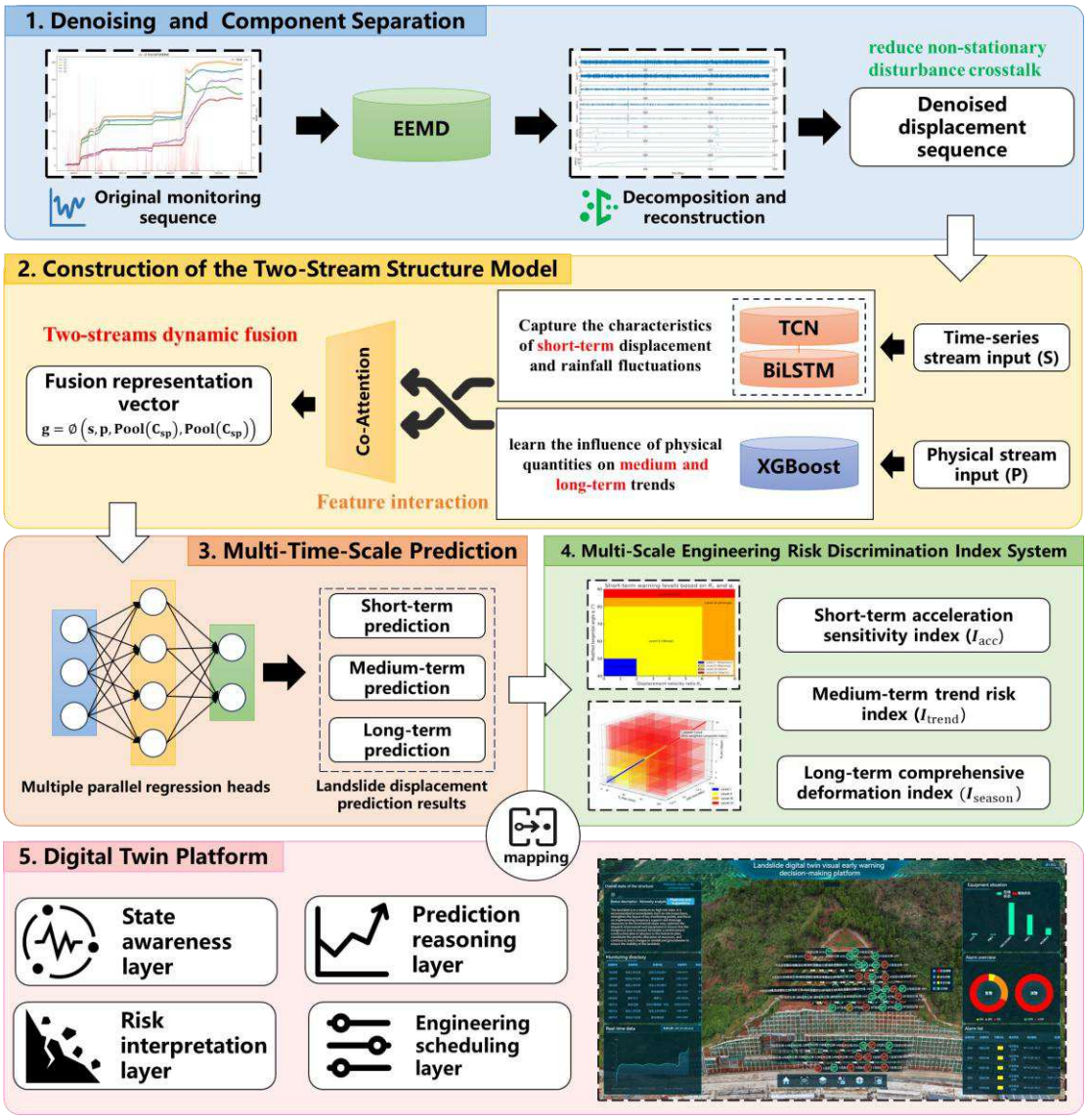


Fig.1 Full-cycle landslide prediction and intelligent risk decision-making framework driven by dual-flow deep learning model

2. Literature Review

With advances in monitoring technologies, data-processing capabilities, and intelligent computation, traditional landslide disaster-mitigation practices are increasingly inadequate. In

121 engineering applications, unstable identification of short-term acceleration phases, long-term
122 trend drift leading to false or missed alarms, and the lack of systematic linkage between
123 warning thresholds and engineering response workflows collectively hinder reliable risk
124 reduction. Among existing approaches, displacement prediction based on sensor monitoring
125 remains the most direct and widely used method for early hazard identification and risk
126 control. Research in this field has undergone multiple stages of evolution—from empirical
127 statistical models and numerical analysis to machine-learning–based intelligent prediction[18].
128 Early studies predominantly relied on statistical regression and classical time-series analysis.
129 Saito (1969) [19] proposed a three-stage creep model for forecasting slope failure time, while
130 Fukuzono (1985) [20] introduced the inverse-velocity method to estimate failure time during
131 the accelerating deformation phase. Together, these seminal works laid the foundation for
132 subsequent landslide-displacement prediction research. Hoek and Bray's (1977) limit-
133 equilibrium analysis[21] and Cruden's (1996) displacement-based classification system[22]
134 further revealed the physical mechanisms underlying landslide deformation. Although these
135 studies offered strong interpretability, their predictive accuracy was inherently limited. Since
136 the early 21st century, statistical and time-series models have been increasingly incorporated
137 into landslide prediction. Xie et al. (2005) [23] applied a modified grey model GM(1,1) to
138 capture displacement trends. Dong et al. (2007)[24] developed a Boosting-based support
139 vector regression framework to improve prediction performance. Yin et al. (2009)[25]
140 employed ARIMA to analyze coseismic landslides induced by the Wenchuan earthquake,
141 demonstrating its applicability to nonstationary sequences. While these methods are capable
142 of modeling certain nonlinear relationships, they fall short in representing long-term

deformation evolution and the interactions among multiple driving factors. With further improvements in monitoring resolution and computational power, machine-learning methods have gained prominence in landslide prediction. Pradhan (2012) [26] used decision trees and neuro-fuzzy models for hazard susceptibility assessment. Pham et al. (2015)[27] applied least-squares support vector machines (LSSVM) and multiclass alternating decision trees (MADT), achieving better accuracy than traditional linear models. Deep learning has further accelerated methodological advances. Liu et al. (2020)[28] modeled “step-like” displacement patterns in the Three Gorges Reservoir area using LSTM and GRU, demonstrating deep networks’ strengths in capturing periodic deformation. Jiang et al. (2020)[29]combined LSTM and SVR via optimal weighting to enhance prediction precision. Azarafza et al. (2021)[30] constructed a CNN–DNN architecture for landslide susceptibility mapping, outperforming several benchmark models. Nava et al. (2023) [31] systematically compared deep-learning architectures and found convolution–recurrent hybrids to be most effective for seasonal landslides, whereas MLP and LSTM models perform sufficiently well for slow-moving creep landslides. Despite these advances, most existing models rely heavily on displacement as a single input variable, making them susceptible to limited generalization under complex and multi-source environmental disturbances. As highlighted by Gong et al. (2024) [1] , purely data-driven models offer strong short-term fitting capability but remain insufficient in capturing environmental triggers and underlying physical mechanisms, thereby restricting both interpretability and stability. To enhance prediction stability and interpretability, research has gradually shifted from single-variable displacement modeling toward integrated frameworks combining multi-scale decomposition and physical information. The Empirical

Mode Decomposition (EMD) proposed by Huang et al. (1998) [32]established the foundation for multi-component analysis of landslide signals. Wu and Huang's (2009)[33]Ensemble EMD (EEMD) further alleviated mode mixing, enabling more reliable component separation. Building on these advances, hybrid models such as VMD–LSTM have been shown to achieve superior performance on noisy signals (Taorui, 2022) [34] . More recently, Wang et al. (2024) [35] coupled VMD with rainfall data and an optimized LSTM to realize high-precision real-time displacement prediction, while Zhou (2025)[36] developed an interpretable trend–seasonal–noise decomposition framework using VMD combined with ARIMA, BiGRU, and attention mechanisms However, prediction frameworks relying solely on displacement signals remain vulnerable to instability in complex environmental settings. To strengthen physical consistency, Physics-Informed Neural Networks (PINNs) and related extensions have attracted increasing attention (Karniadakis et al., 2021[37] ; Raissi et al., 2019[38]）. In landslide studies, Ma et al. (2023)[39] embedded domain knowledge into deep models to enhance engineering interpretability, whereas Chen et al. (2024)[40] proposed ω-GNN/ω-EGNN architectures that incorporate physical variables and climatic constraints, achieving more robust predictive performance. Meanwhile, advances in monitoring technologies have made multi-source data fusion a dominant research direction. Carlà et al. (2018)[41] were the first to jointly employ multi-temporal InSAR and ground-based radar for hazard assessment. Jin et al. (2022)[42] and Hu et al. (2025)[43] further demonstrated that integrating topographic, geological, hydrological, and InSAR-derived features significantly improves landslide detection and spatial prediction accuracy. Although notable progress has been made in signal decomposition, statistical learning, and deep modeling, substantial gaps remain in achieving multi-timescale

consistency, embedding physical constraints, and ensuring cross-scenario transferability. Against this backdrop, this study introduces a co-attention dual-stream framework that integrates temporal features with physical priors to achieve full-cycle displacement prediction—from short-term responses to medium- and long-term evolution—offering a scalable pathway for intelligent landslide early warning and engineering risk management.

In current engineering practice, displacement-driven criteria remain the predominant basis for landslide early warning. The *Code for Investigation of Landslide Prevention Engineering* (GB 32864-2016) [44] and the *Specifications for Monitoring of Collapse, Landslide and Debris Flow* (DZ/T 0221-2006) [45] explicitly stipulate that displacement magnitude and velocity should serve as key indicators for evaluating slope stability and assigning warning levels. The *Technical Specification for Geological Disaster Monitoring and Early Warning in Sichuan Province* (DB51T3302-2025)[46] provides a guideline for threshold setting in soil landslide warning, emphasizing the use of displacement–time curves, tangential-angle variation, and deformation-stage identification to classify creeping, steady, accelerating, and pre-failure phases. Regarding specific criteria, Cruden and Varnes (1996) [22] proposed a velocity-based landslide classification system that divides displacement into seven categories and demonstrates a positive correlation between hazard severity and velocity level. Xu Qiang et al. (2009)[47] introduced an improved tangential-angle method for quantitatively identifying creeping, steady, accelerating, and imminent-failure stages, which has become one of the most widely applied approaches for pre-failure recognition. Wang Liwei et al. (2014)[48] proposed the displacement rate–ratio method, which characterizes the relative activity of a monitoring point using the ratio between current and baseline rates. Building on this, Ben Yanqi et al.

(2023)[49] developed a multi-criteria warning framework integrating rate ratio, effective rainfall, and improved tangential angle. Huang Xiaohu et al. (2018)[50] established progressively graded warning intervals based on daily rainfall and daily displacement rate using specific engineering case studies. Georgieva et al. (2012)[51] summarized the relationship between inverse velocity and time-to-failure, forming the classical framework for acceleration-phase identification and failure-time extrapolation. More recently, the Comprehensive Standard Deformation Index (CSDI)[52] has been introduced, which normalizes displacement, velocity, and other indicators, applies probability-distribution analysis, and derives a unified index to quantify medium- to long-term trend risk.Building on these standards, theories, and engineering practices, this study develops a set of three time-scale-specific indicators—short-term acceleration-sensitivity index, medium-term trend-risk index, and long-term integrated deformation index—based on the model-predicted multi-timescale displacement series, enabling systematic mapping from physically meaningful deformation metrics to engineering warning levels.

With advances in displacement prediction and risk classification, landslide early warning is increasingly evolving toward systematized and intelligent decision-making. Piciullo et al. (2025) [53] proposed a digital twin–driven slope stability forecasting framework that integrates real-time monitoring data, meteorological information, and numerical models to construct an automated IoT-based local landslide early-warning system. Xu and Zhang (2025)[54] developed an AI-enhanced digital-twin framework that fuses LiDAR and other multi-source data to generate high-resolution 3D slope models and employ machine learning for real-time landslide risk prediction. Li Xiaomeng et al. (2024)[55] applied digital-twin technology to

submarine geohazards, developing a real-time monitoring–based digital twin for subsea engineering geological systems to support dynamic simulation and early warning. Tong Bin et al. (2025) [56] explored the application of large AI models in geohazard assessment and slope-engineering decision support, highlighting their potential as intelligent assistants. Building upon these developments, this study proposes a digital twin–enabled multi-timescale engineering decision-making framework for landslides. By integrating displacement prediction, risk classification, and real-time monitoring data, the system realizes a fully closed loop encompassing short-term acceleration response, medium-term trend assessment, and long-term deformation evaluation. Incorporating digital-twin and numerical-simulation technologies into conventional physical-indicator–based approaches, the framework provides high-precision, interpretable, and cross-scenario scalable full-cycle decision support for landslide prevention and mitigation.

3. Time series + physical dual-flow deep learning landslide displacement prediction model

3.1 Model architecture

This study proposes a multi-timescale landslide displacement forecasting method based on a temporal–physical dual-stream architecture. The approach takes monitored displacement time series as the primary data source and employs Ensemble Empirical Mode Decomposition (EEMD) for signal denoising and component decomposition. A dual-stream predictive framework is then constructed, consisting of a temporal stream and a physical stream. The two streams are dynamically linked through a co-attention mechanism, enabling coordinated forecasting of short-term and medium- to long-term displacement across multiple timescales. The complete model comprises six functional modules: an input preprocessing module, an

EEMD-based decomposition and reconstruction module, a temporal-stream modeling module, a physical-stream modeling module, a dual-stream fusion module, and a multi-timescale prediction module. The overall workflow of the proposed method is illustrated in Fig. 2.

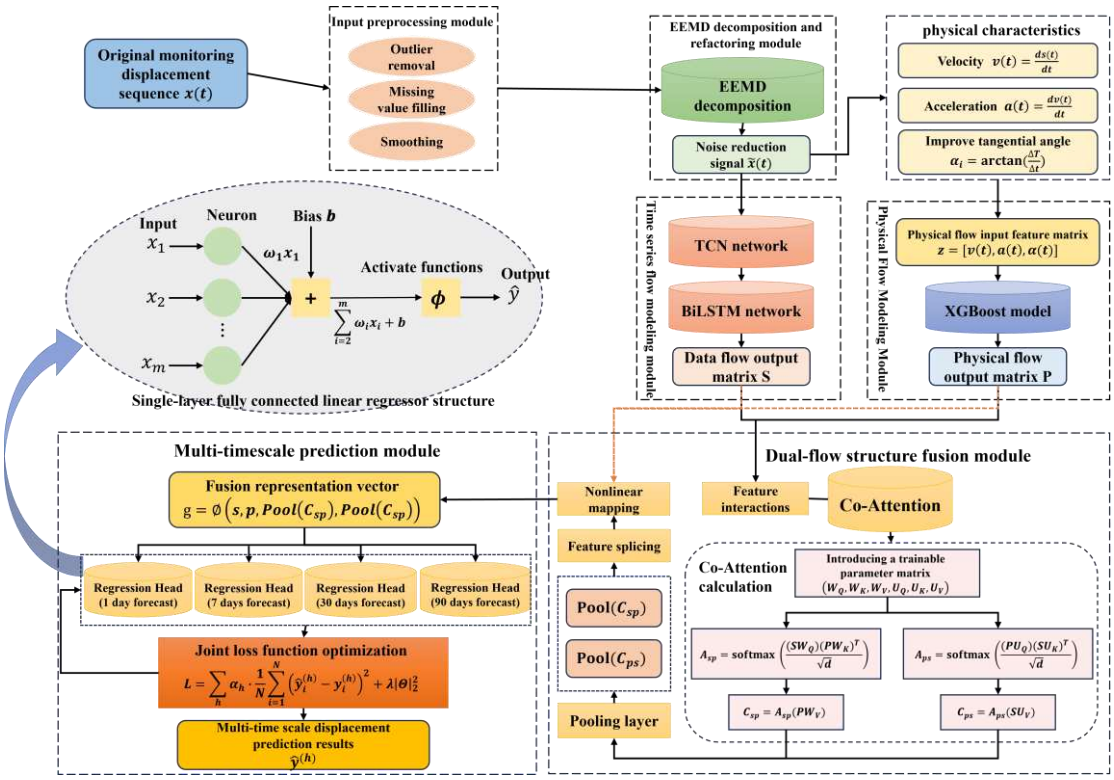


Fig. 2. Flow of Landslide Displacement Prediction Method Based on Temporal-Physical Dual-Stream Structure Model.

3.1.1 Processing of Temporal and Physical Data

The raw displacement time series $x(t)$obtained from field monitoring are first subjected to outlier removal, missing-value imputation, and smoothing. Following preprocessing, Ensemble Empirical Mode Decomposition (EEMD) is applied to achieve multi-scale signal decomposition. EEMD extends the conventional Empirical Mode Decomposition (EMD) by introducing an ensemble of added white-noise perturbations, thereby alleviating mode mixing and improving decomposition robustness. The detailed procedure is illustrated in Fig. 3.

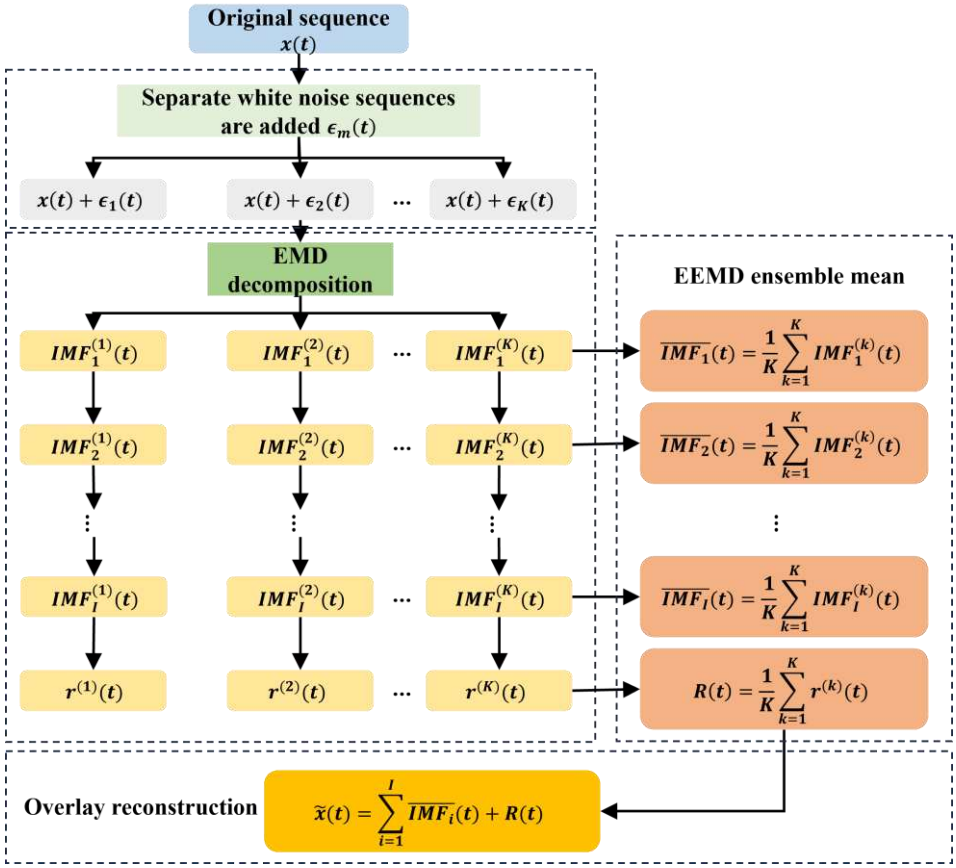


Fig. 3. Flow of Ensemble Empirical Mode Decomposition (EEMD) Algorithm.

For the original displacement sequence $x(t)$, multiple independent Gaussian white-noise sequences $\varepsilon_k(t)$ are added to construct an ensemble. Each noise-augmented sequence is then decomposed using EMD to obtain the intrinsic mode function (IMF) components $\mathrm{IMF}_i^{(k)}(t)$ for the k-th realization. The final, noise-robust IMF components are obtained by averaging across all ensemble realizations:

$$\overline{IMF_i}(t)=\frac{1}{K}\sum_{k=1}^{K}IMF_i^{(k)}(t) \tag{1}$$

Using the averaged IMF components, the denoised displacement signal is reconstructed as：

$$\tilde{x}(t)=\sum_{i=1}^{I}\overline{IMF_i}(t)+r(t) \tag{2}$$

where $r(t)$ denotes the residual term. The EEMD procedure effectively suppresses high-frequency fluctuations while preserving low-frequency trends, thereby providing a more

stable and informative input for subsequent deep-learning–based modeling.

Three physical feature quantities derived from the displacement sequence are then computed, namely velocity $v(t)$, acceleration $a(t)$, and the improved tangential angle $\alpha(t)$. Velocity and acceleration are obtained using first-order and second-order finite differences, respectively:

$$v(t) = \frac{ds(t)}{dt} \tag{3}$$

$$a(t) = \frac{dv(t)}{dt} \tag{4}$$

To more accurately characterize the transition of the landslide mass from deceleration to acceleration, an improved tangential angle α_i is introduced. The displacement–time curve $S(t)$ is normalized using the displacement rate v during the quasi-steady stage to construct a normalized cumulative displacement curve $T(i) = S(i)/v$. The improved tangential angle at monitoring time t_i is defined as the slope angle of the tangent to this curve:

$$\alpha_i = \arctan\left(\frac{T(i) - T(i-1)}{t_i - t_{i-1}}\right) = \arctan\left(\frac{\Delta T}{\Delta t}\right) \tag{5}$$

These three physical quantities collectively form the input feature matrix of the physical stream, capturing the dynamical characteristics of landslide deformation across different evolutionary stages.

3.1.2 Construction of the Dual-Stream Architecture

The proposed dual-stream architecture consists of a temporal stream and a physical stream. The temporal stream takes the EEMD-denoised displacement sequence as input and employs a cascaded structure combining a TCN and a BiLSTM to extract temporal dependency features.

The overall structure of the temporal stream is illustrated in Fig. 4.

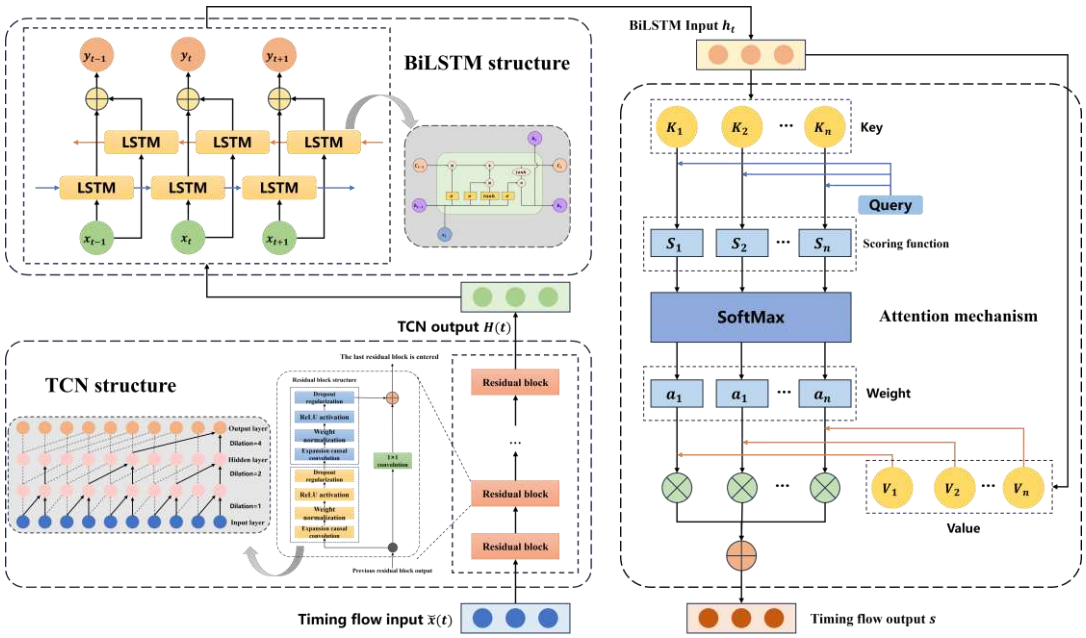


Fig. 4. Structure of Temporal Stream Model Based on TCN-BiLSTM.

(1) Temporal Stream

The TCN module adopts one-dimensional causal dilated convolutions, where the dilation factor increases layer by layer to enlarge the receptive field and capture local fluctuation patterns of landslide displacement. The computation is expressed as：

$$H^{(l)} = \sigma\left(BN(H^{(l-1)} *_{d_l} W^{(l)} + b^{(l)})\right) + H^{(l-1)} \tag{6}$$

where $*_{d_l}$ denotes a causal convolution with dilation rate d_l, BN is batch normalization, and $\sigma(\cdot)$ is a nonlinear activation function. This structure preserves temporal causality while enabling stable information propagation through deep residual connections. The output of the TCN is then passed to a BiLSTM module for global temporal dependency modeling. The forward and backward hidden states are computed as：

$$\vec{\mathbf{h}}_t = \mathrm{LSTM}_f(\mathbf{H}_t, \vec{\mathbf{h}}_{t-1}) \tag{7}$$

$$\overleftarrow{\mathbf{h}}_t = \mathrm{LSTM}_b(\mathbf{H}_t, \overleftarrow{\mathbf{h}}_{t+1}) \tag{8}$$

313 And concatenated to form the hidden vector $\mathbf{h}_t = [\vec{\mathbf{h}}_t; \overleftarrow{\mathbf{h}}_t]$。 An attention-weighted pooling

314 mechanism is applied to obtain the global temporal representation:

315 $$\alpha_t = \frac{\exp(w^T h_t)}{\sum_k \exp(w^T h_k)} \tag{9}$$

316 $$s = \sum_t \alpha_t h_t \tag{10}$$

317 The temporal-stream output $s$thus integrates short-term fluctuation patterns with long-range

318 dependencies.

319 **(2) Physical Stream**

320 The physical stream takes three physical indicators—velocity $v(t)$, acceleration $a(t)$, and

321 improved tangential angle $\alpha(t)$—as input and employs an XGBoost model to learn nonlinear

322 mappings and embed physical constraints. XGBoost constructs an additive ensemble of

323 regression trees:

324 $$\hat{y} = \sum_{m=1}^{M} f_m(\mathbf{z}), \quad f_m \in \mathcal{F} \tag{11}$$

325 where $z = [v(t), a(t), \alpha(t)]$is the input vector, $f_m(\cdot)$denotes the m-th regression tree, and

326 $\mathcal{F}$is the space of CART trees. The model is optimized by minimizing:

327 $$\mathcal{L}_{\text{xgb}} = \sum_i \ell(y_i, \hat{y}_i) + \sum_m \Omega(f_m) \tag{12}$$

328 where $l(\cdot)$is the squared-error loss and $\Omega(\cdot)$is a regularization term preventing overfitting. At

329 each iteration, XGBoost uses a second-order Taylor expansion of the loss and fits residuals to

330 update model parameters. The resulting output is a physical-constraint vector $p \in \mathbb{R}^q$, where

331 each dimension corresponds to a nonlinear representation of landslide dynamical

332 characteristics.

333 In this physical stream, velocity $v(t)$ describes instantaneous displacement trends,

acceleration $a(t)$reflects dynamic responses during acceleration phases, and the improved tangential angle $\alpha(t)$characterizes local deviations in displacement growth rate and potential instability. Together, these features form an interpretable and physically meaningful representation of landslide evolution. The physical-stream output p interacts with the temporal-stream output $s$in the subsequent fusion stage.

(3) Dual-Stream Fusion via Co-Attention

To enable bidirectional information exchange between the temporal and physical streams, a co-attention mechanism is introduced. This mechanism computes similarity matrices between temporal features and physical features, generating two sets of attention weights. Let $S \in \mathbb{R}^{T\times d_s}$denote the temporal-stream output matrix and $P \in \mathbb{R}^{T\times d_p}$the physical-stream output matrix. The co-attention computations are given by:

$$A_{sp} = \mathrm{softmax}\left(\frac{(SW_Q)(PW_K)^T}{\sqrt{d}}\right), \qquad C_{sp} = A_{sp}(PW_V) \tag{13}$$

$$A_{ps} = \mathrm{softmax}\left(\frac{(PU_Q)(SU_K)^T}{\sqrt{d}}\right), \qquad C_{ps} = A_{ps}(SU_V) \tag{14}$$

where $W_Q, W_K, W_V, U_Q, U_K, U_V$are learnable projection matrices. A_{sp}denotes the attention distribution from temporal features to physical features, while A_{ps}represents the reverse. Through this design, the model adaptively strengthens the sensitivity of displacement predictions to physical changes, particularly during acceleration phases, and maintains dominant factor awareness across different deformation stages (stable–transition–accelerated).

The fused representation is obtained by pooling and concatenating the attended features:

$$g = \phi\left([s, p, \mathrm{Pool}(C_{sp}), \mathrm{Pool}(C_{ps})]\right) \quad (15)$$

where $\phi(\cdot)$ is a nonlinear transformation composed of fully connected layers, activation functions, and normalization operations. The fusion vector g jointly preserves temporal dependencies and physical constraints and serves as the unified input for multi-timescale prediction.

(4) Multi-Timescale Prediction Head

The multi-timescale prediction module consists of several parallel regression heads, corresponding to forecasting horizons of 1, 3, 7, 30, and 90 days. Each head is formulated as a single fully connected linear regressor:

$$\hat{y}^{(h)} = \mathbf{w}_h^{\top}\mathbf{g} + b_h, \quad h \in \{1,3,7,30,90\} \quad (16)$$

Model training is performed using a joint loss function integrating all timescales:

$$\mathcal{L} = \sum_h \alpha_h \cdot \frac{1}{N}\sum_{i=1}^{N}(\hat{y}_i^{(h)} - y_i^{(h)})^2 + \lambda|\Theta|_2^2 \quad (17)$$

where $\boldsymbol{\alpha_h}$ is the loss weight for each horizon, $\boldsymbol{\lambda}$ is the regularization coefficient, and $\boldsymbol{\Theta}$ denotes all learnable parameters. Optimization is carried out using the Adam algorithm with adaptive learning rate scheduling and early stopping. After training, the model simultaneously outputs displacement forecasts across all timescales in a single forward pass.

3.2 Case studies and model evaluation

3.2.1 Scenario Background and Prediction Requirements

To evaluate the applicability of the proposed temporal–physical dual-stream model to complex rainfall-induced landslides, the Zaoshuwa landslide in Yunxi County, Shiyan City, Hubei Province, is selected as a representative case. This medium-scale colluvial landslide features loose material structure and high permeability, exhibiting a cyclic deformation pattern

characterized by slow creeping, accelerated movement, and short-term stabilization. The G1 point, located at the leading edge of the main slip zone, displays the most active displacement and pronounced rainfall sensitivity, making it the critical early-warning indicator. Five GNSS displacement monitoring stations (G1–G5) were installed along the main cross-section, with a sampling interval of 1 hour over a monitoring period of approximately 20 months. The observed data exhibit clear nonstationary characteristics, including long-term creeping trends, seasonal fluctuations, and high-frequency disturbances (Fig. 4). Engineering concerns center on both short-term acceleration response and medium- to long-term risk assessment. In this study, points G2–G5 are used as the training set, while G1 is used as the validation set to mimic the engineering scenario in which the relatively stable region informs the overall deformation mechanism, while predictions target the sensitive frontal zone. This setup enables a systematic evaluation of the model's stability and reliability in cross-spatial prediction and multi-timescale forecasting.

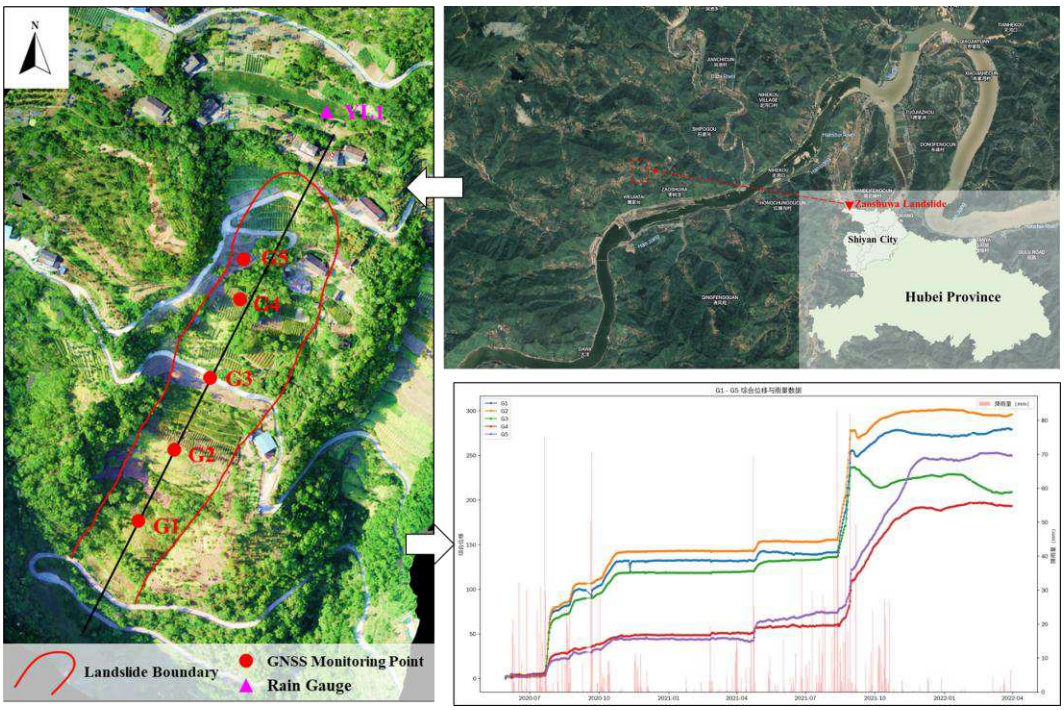


Fig. 5. Overview Map of Zaoshuwa Landslide.

3.2.2 Data Processing and Construction of Physical Features

To characterize the nonstationary behavior of landslide displacement and its time-varying sensitivity to rainfall, daily displacement series from monitoring points G1–G5 were preprocessed and feature-engineered. First, Ensemble Empirical Mode Decomposition (EEMD) was applied to decompose each sequence into intrinsic mode functions (IMFs). Low-frequency IMFs and the residual component were retained and reconstructed to suppress high-frequency disturbances and background noise, thereby separating short-term fluctuations from long-term deformation trends (illustrated using G1 in Fig. 6). Based on the reconstructed displacement, physical descriptors—including displacement velocity v_t, acceleration a_t, and the improved tangential angle α_t—were extracted to capture the staged evolution from creeping to acceleration and post-peak stabilization. The final model input consists of both reconstructed temporal features and structured physical variables, providing a comprehensive data foundation for the dual-stream cooperative framework.

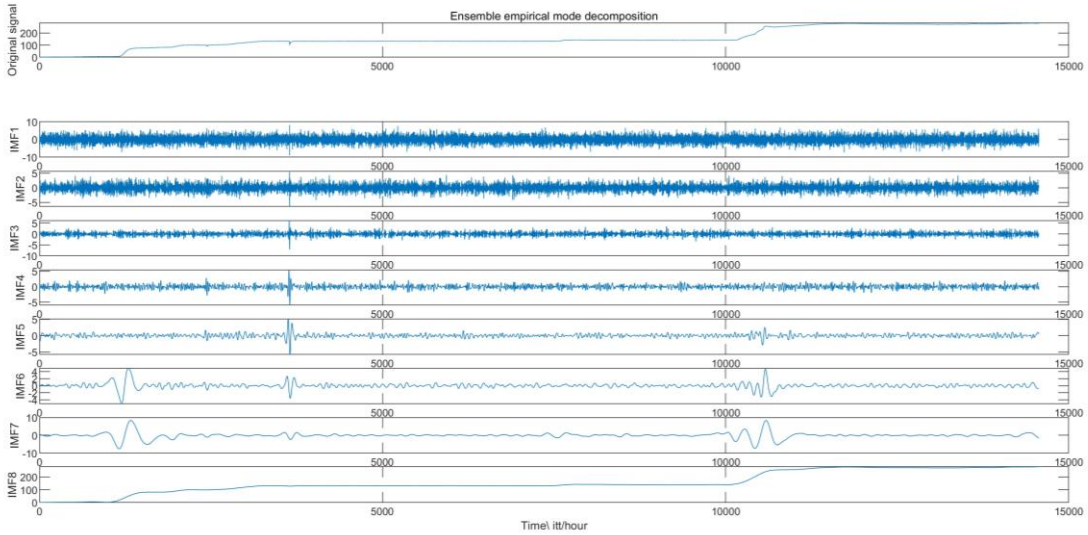


Fig. 6. Results of Ensemble Empirical Mode Decomposition for G1 Monitoring Point.

3.2.3 Training of the Dual-Stream Model

To evaluate the predictive capability of the dual-stream architecture, the EEMD-reconstructed displacement series from G2–G5 were used as the training dataset. The physical branch incorporated velocity, acceleration, and improved tangential angle as structured inputs to form a complete feature system. A sliding-window method was used to generate 3-day input–output training pairs. Model training employed the Adam optimizer with an initial learning rate of 1×10^{-3}, and an early-stopping strategy was implemented to prevent overfitting.The 3-day forecasting results (Fig. 7) demonstrate that the dual-stream architecture performs robustly across both gradual and accelerating deformation phases. The model successfully anticipates rainfall-triggered acceleration inflection points, significantly reducing short-term prediction errors (RMSE = 4.1081, MAE = 2.9971, MAPE = 1.9578%, $R^2 = 0.99733$). These results indicate that the model maintains excellent fitting performance even under high-frequency disturbance conditions.

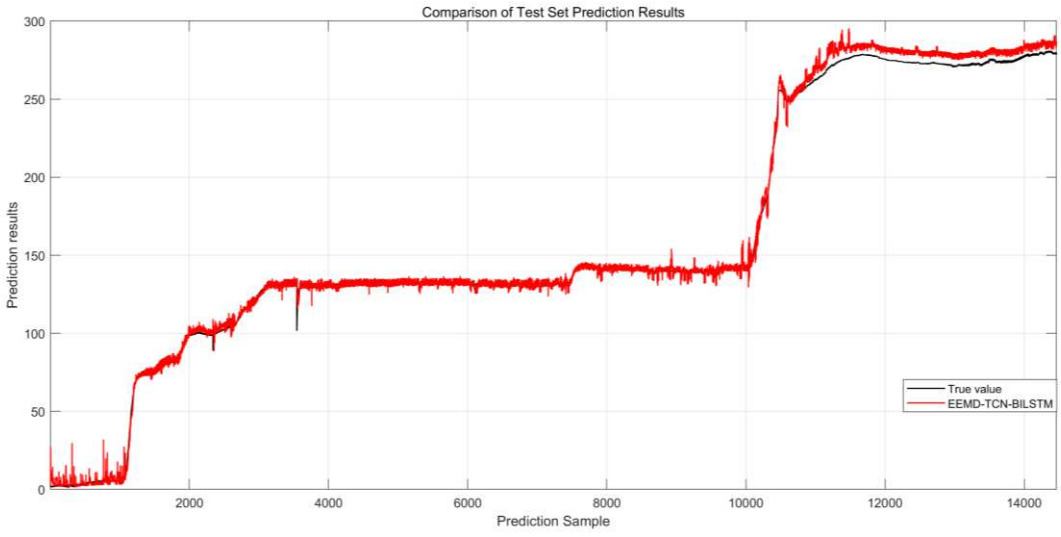


Fig. 7. Prediction Results of Dual-Stream Structure Model.

To evaluate the influence of rainfall as an external driving factor, two comparative models were constructed: one incorporating rainfall input and one excluding it. The results (Fig. 8) show

that, without rainfall information, the model substantially underestimates both major acceleration phases and exhibits a delayed response (R^2 = 0.9621, RMSE = 15.4863). In contrast, when rainfall series are included, the model successfully captures rainfall-triggered acceleration processes and significantly improves short-term prediction accuracy. This comparison indicates that rainfall, as a key external driver, directly governs the model's sensitivity to acceleration events.

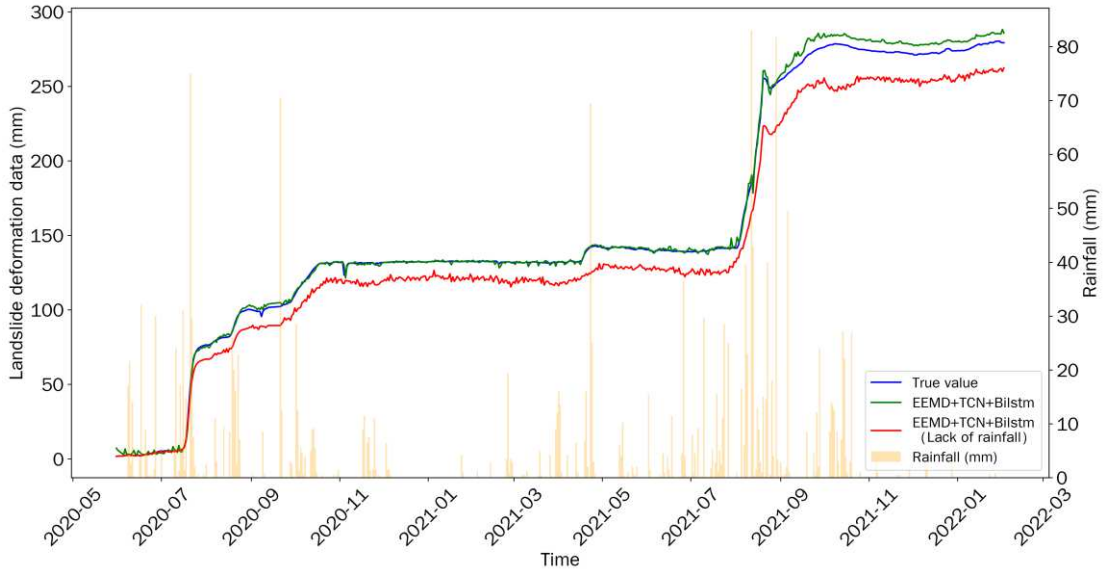


Fig. 8. Comparison of Dual-Stream Structure Model Prediction Results with and without Rainfall.

In addition, a single-stream model relying solely on temporal features—without physical variables—was developed as a control. As shown in Fig. 9, the absence of physical descriptors weakens the model's ability to recognize staged deformation behavior. In particular, both major acceleration phases are notably underestimated and delayed. Prediction errors on the test set increase significantly: RMSE reaches 13.8, MAE is 12.8088, MAPE rises to 6.8493%, and the coefficient of determination drops to 0.96989. These results demonstrate that, without physical constraints, the model struggles to accurately reconstruct the true

deformation profile during acceleration phases.

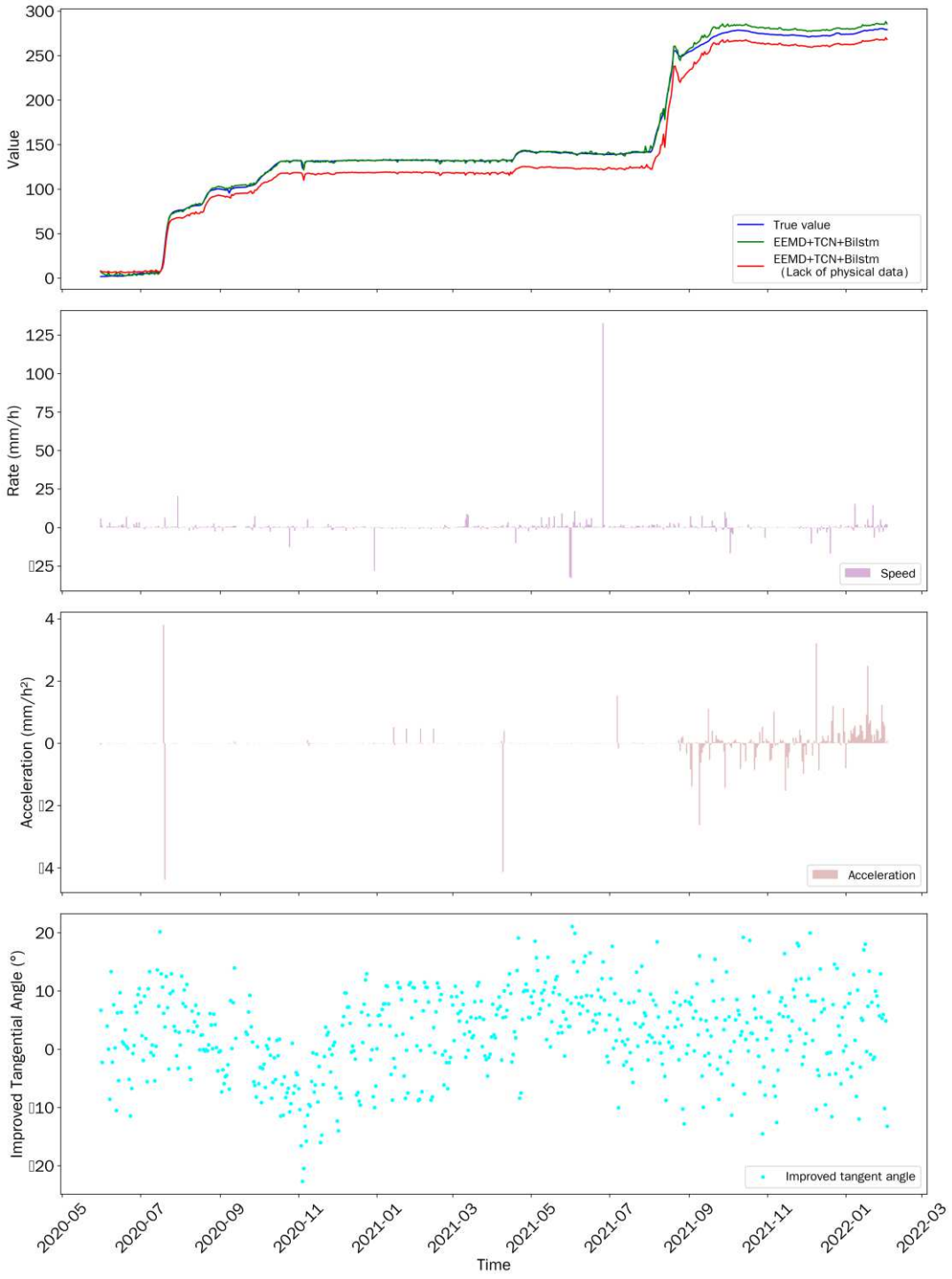


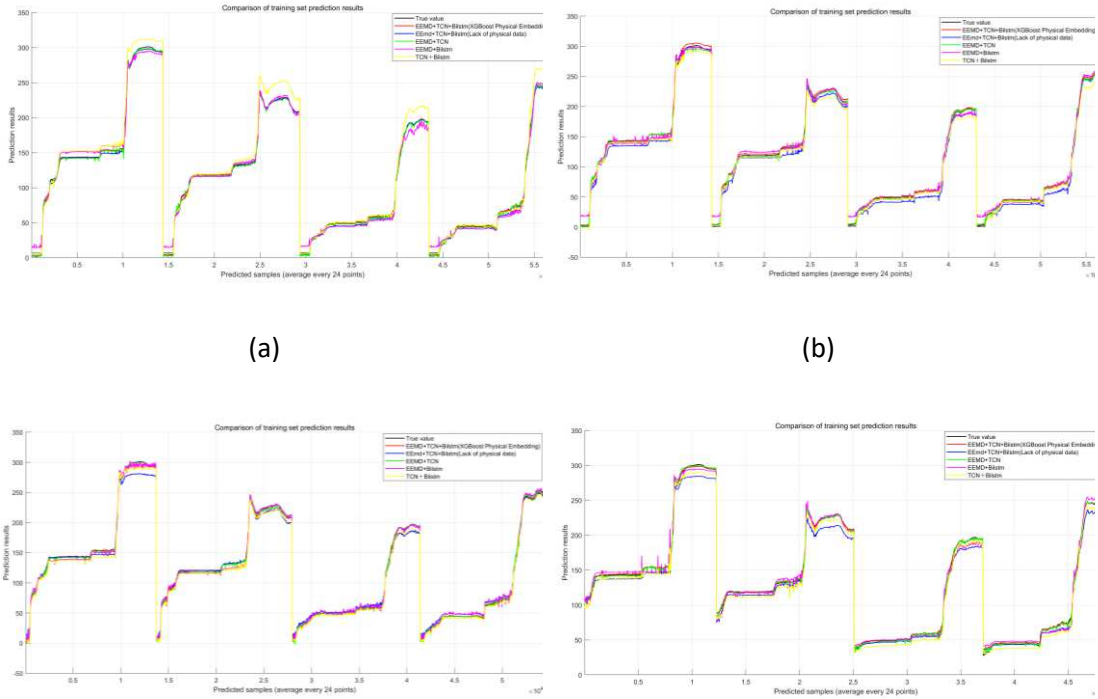
Fig. 9. Comparison of Prediction Results with and without Physical Features.

Overall, the prediction results demonstrate that the dual-stream architecture performs effectively in integrating multi-scale temporal features with dynamical physical information. The model provides consistent responses during rainfall-triggered acceleration phases while

maintaining stable trend characterization during gradual deformation intervals, resulting in predicted displacement trajectories that align more closely with actual observations throughout the entire evolution process. These results indicate that jointly modeling temporal information and physical features contributes significantly to improving the overall reliability of landslide prediction.

3.2.4 Multi-Timescale Prediction and Comparative Analysis

To systematically evaluate the stability and adaptability of the proposed dual-stream model across various forecasting horizons, four prediction tasks were constructed: 1-day, 7-day, 30-day, and 90-day forecasts. Comparative experiments were performed against five benchmark architectures: EEMD + TCN + BiLSTM, EEMD + TCN + BiLSTM (without physical features), EEMD + TCN, EEMD + BiLSTM, and TCN + BiLSTM. All baseline models were independently trained using the same training–testing split to ensure fair comparison. Representative training-set results are shown in Fig. 10.



(a) (b)

(c) (d)

458 **Fig. 10. Comparison of Training Set Results for Multi-Time-Scale Models: (a) 1-Day**

459 **Forecast (b) 7-Day Forecast (c) 30-Day Forecast (d) 90-Day Forecast.**

460 The multi-timescale prediction performance of the proposed dual-stream model is presented

461 in Fig. 11 and Table 1. In short-term forecasting, the model responds sensitively to

462 displacement surges, achieving an RMSE of only 2.35 and an R^2 of 0.999. For medium- and

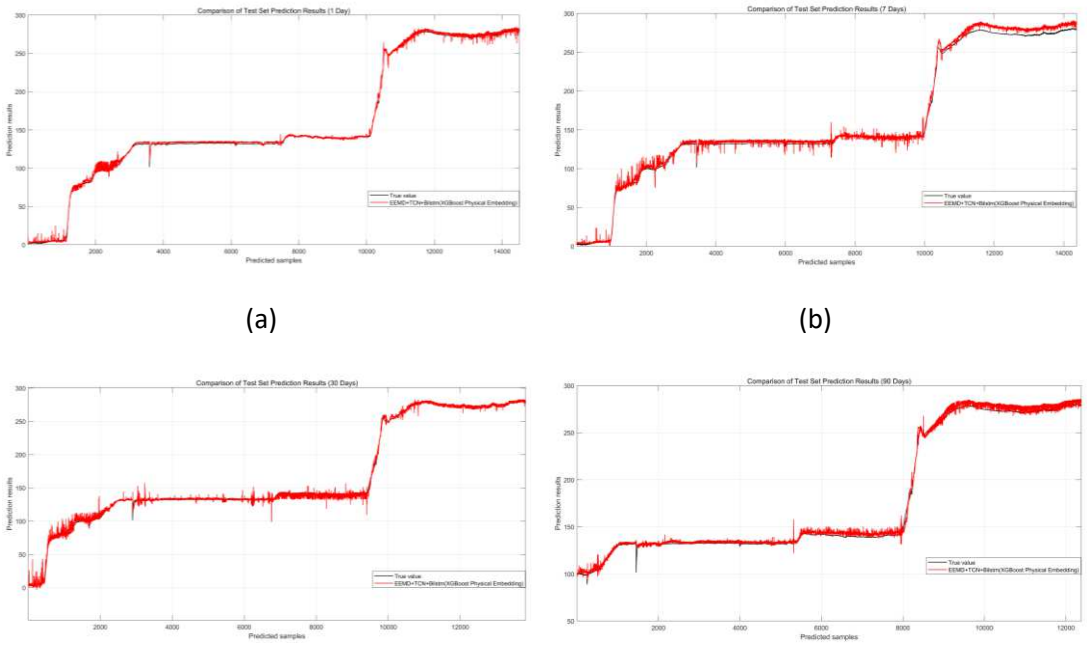
463 long-term forecasting, the model maintains strong consistency with actual displacement

464 trends, with R^2 values exceeding 0.996 across all horizons. These results collectively

465 demonstrate that the proposed model achieves stable performance and high predictive

466 accuracy at multiple timescales, exhibiting strong generalization and enabling unified

467 forecasting from short-term early warning to medium- and long-term trend assessment.



(a) (b)

(c) (d)

468 **Fig. 11. Multi-Time-Scale Prediction Results of Temporal-Physical Dual-Stream Structure**

469 **Model: (a) 1-Day Forecast (b) 7-Day Forecast (c) 30-Day Forecast (d) 90-Day Forecast.**

Table 1. Evaluation Metrics for Multi-Time-Scale Prediction of Temporal-Physical Dual-Stream Structure Model.

Timescale/Error Indicator	RMSE	MAE	MAPE	R^2
1-Day	2.3524	1.8144	0.97599%	0.99913
7-Day	4.8278	3.8275	2.4014%	0.99624
30-Day	3.3116	2.174	1.0013%	0.99798
90-Day	3.6916	2.8956	1.6058%	0.99685

(1) 1-Day Forecasting Horizon

In the 1-day prediction task, notable differences emerge among the five models in terms of fitting accuracy and responsiveness to staged deformation. As shown in Fig. 12 and Table 2, the dual-stream EEMD + TCN + BiLSTM (with physical information) exhibits the highest consistency with the observed displacement, closely tracking the two major acceleration surges and maintaining a stable, drift-free trajectory during the plateau periods. It achieves the lowest testing error among all models.The single-stream variant without physical features captures the general trend but shows slight lag during acceleration phases and mild underestimation during the plateau stages (RMSE increases to 4.2043). EEMD + TCN and EEMD + BiLSTM perform moderately well; the former amplifies local noise under high-frequency fluctuations, while the latter exhibits noticeable deviation near acceleration points, corresponding to RMSE values of 4.1248 and 6.7086, respectively. The TCN + BiLSTM model performs the worst, significantly overestimating displacement in both surge events, with the largest overall deviation (RMSE = 14.3771, R^2 = 0.96763).

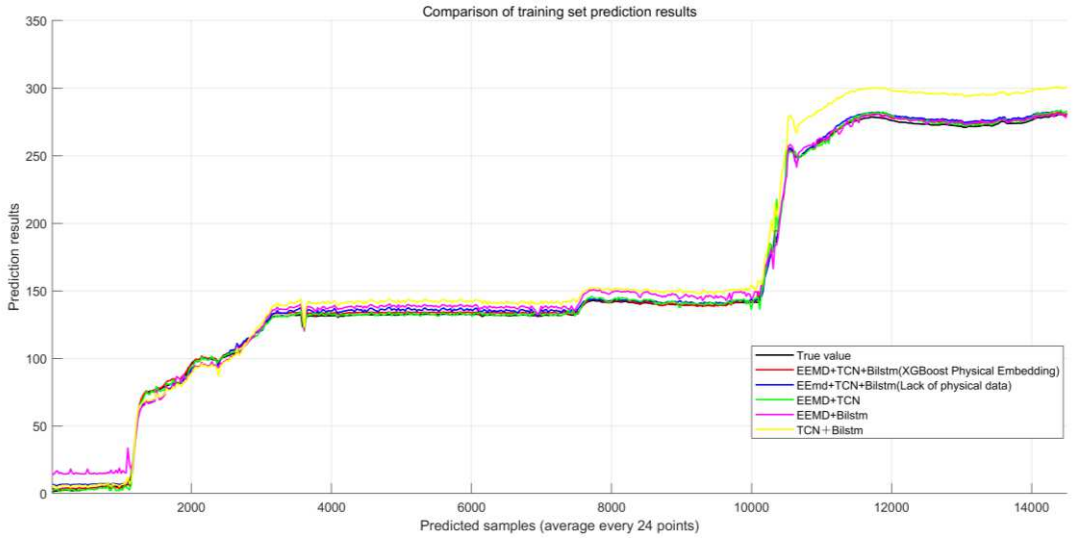


Fig. 12. Comparison of Different Models' Prediction Results at the 1-Day Time-Scale.

Table 2. Evaluation Metrics of Different Models' Prediction at the 1-Day Time-Scale.

Models	RMSE	MAE	MAPE	R^2
EEMD+TCN+BiLSTM (with Physical Information Embedding)	2.3524	1.8144	0.97599%	0.99913
EEMD+TCN+BiLSTM (without Physical Information Embedding)	4.2043	3.394	1.735%	0.99723
EEMD+TCN	4.1248	2.9461	1.612%	0.99734
EEMD+BiLSTM	6.7086	5.6055	2.3322%	0.99295
TCN＋BiLSTM	14.3771	12.1336	7.8465%	0.96763

(2) 7-Day Forecasting Horizon

In the 7-day forecast, discrepancies among the models become more pronounced (Fig. 13, Table 3), especially in their ability to extrapolate deformation trends during major acceleration phases. The dual-stream model maintains close alignment with the observed trajectory across both surge and plateau intervals, with minimal fluctuation. In contrast, the single-stream

model (without physical features) demonstrates pronounced underestimation and lag during acceleration stages, with RMSE rising to 8.5756—more than double that of the dual-stream model—highlighting the importance of physical variables in constraining deformation trends. EEMD + TCN exhibits relatively strong performance (RMSE = 4.9979), capturing the overall pattern well, though local deviations are observed in the plateau period.

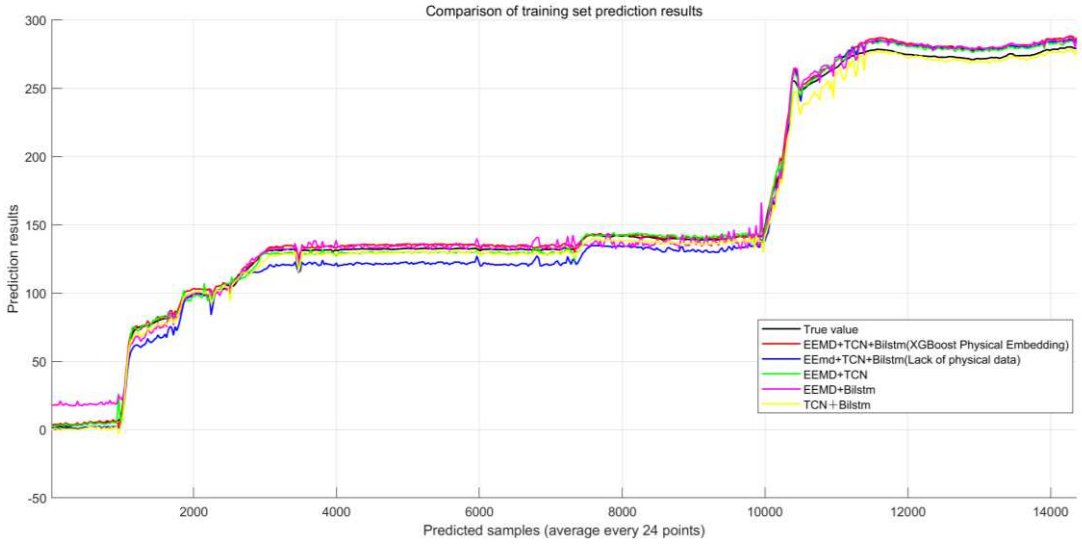


Fig. 13. Comparison of Different Models' Prediction Results at the 7-Day Time-Scale.

Table 3. Evaluation Metrics of Different Models' Prediction at the 7-Day Time-Scale.

Models	RMSE	MAE	MAPE	R^2
EEMD+TCN+BiLSTM (with Physical Information Embedding)	4.8278	3.8275	2.4014%	0.99624
EEMD+TCN+BiLSTM (without Physical Information Embedding)	8.5756	7.6817	3.7659%	0.98814
EEMD+TCN	4.9979	3.6763	2.1162%	0.99597
EEMD+BiLSTM	8.0182	6.4965	3.1416%	0.98963
TCN＋BiLSTM	5.5234	4.0211	2.1478%	0.99508

(3) 30-Day Forecasting Horizon

In the 30-day forecasts, the models' trend-extrapolation capabilities are further tested (Fig. 14, Table 4). The dual-stream model continues to maintain a close match to the observed trend, accurately capturing the morphology of both major acceleration phases and maintaining stability during the plateau interval, achieving the highest precision. Removing physical features causes a substantial increase in error for the single-stream model (RMSE = 5.0497), with marked underestimation during plateau segments and lag during acceleration. EEMD + TCN remains stable at the 30-day horizon (RMSE = 4.7715), demonstrating that multi-scale decomposition paired with convolutional structures preserves strong robustness for long-horizon sequences. EEMD + BiLSTM and TCN + BiLSTM gradually deviate from the true displacement trajectory, particularly overestimating the second major surge, with RMSE values of 8.9392 and 8.1036, respectively. These results illustrate that as the prediction horizon extends to the monthly scale, cumulative error effects intensify, amplifying performance differences among models. The dual-stream structure, supported by the joint constraints of temporal and physical information, exhibits superior stability and noise resistance in long-horizon trend prediction.

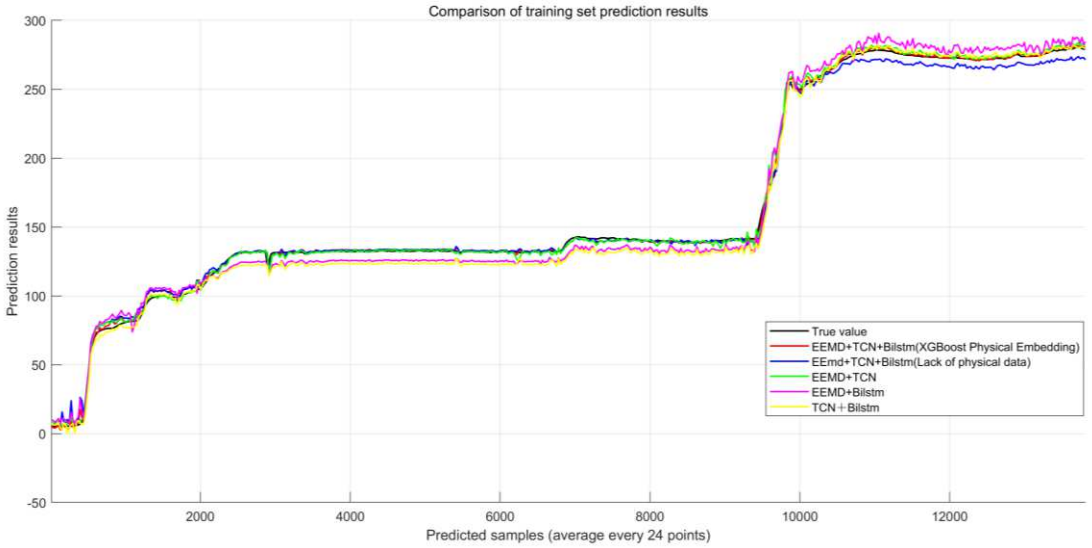


Fig. 14. Comparison of Different Models' Prediction Results at the 30-Day Time-Scale.

Table 4. Evaluation Metrics of Different Models' Prediction at the 30-Day Time-Scale.

Models	RMSE	MAE	MAPE	R2
EEMD+TCN+BiLSTM (with Physical Information Embedding)	3.3116	2.174	1.0013%	0.99798
EEMD+TCN+BiLSTM (without Physical Information Embedding)	5.0497	3.4804	1.9909%	0.9953
EEMD+TCN	4.7715	3.3382	1.7797%	0.99581
EEMD+BiLSTM	8.9392	7.5316	4.0768%	0.98528
TCN＋BiLSTM	8.1036	6.7188	3.1792%	0.98791

(4) 90-Day Forecasting Horizon

In the 90-day forecasts, cumulative errors and trend drift become even more apparent (Fig. 15). The dual-stream model still preserves overall agreement with the true displacement, accurately characterizing the plateau period following the second acceleration event, and maintains the highest accuracy.The single-stream model shows pronounced long-term

deviations, with both underestimation and overestimation in the plateau intervals, indicating that the absence of physical constraints leads to drift in long-horizon trend prediction. EEMD + TCN performs relatively steadily but slightly overestimates the tail of the surge phase. Errors in EEMD + BiLSTM and TCN + BiLSTM further increase (RMSE = 8.6904 and 6.348, respectively), and their long-term trajectories drift significantly.

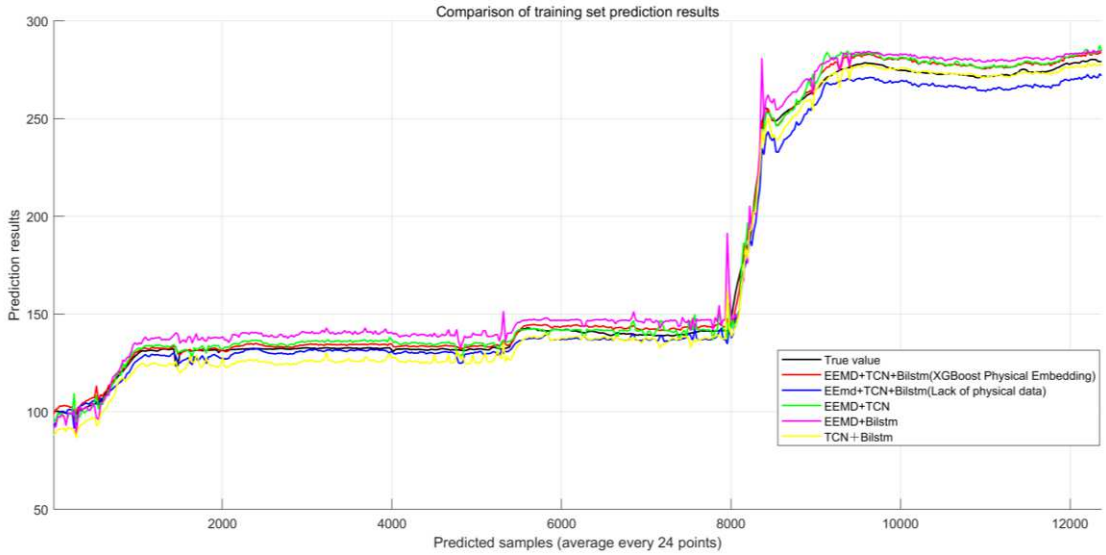


Fig. 15. Comparison of Different Models' Prediction Results at the 90-Day Time-Scale.

Table 5. Evaluation Metrics of Different Models' Prediction at the 90-Day Time-Scale.

Models	RMSE	MAE	MAPE	R2
EEMD+TCN+BiLSTM (with Physical Information Embedding)	3.6916	2.8956	1.6058%	0.99685
EEMD+TCN+BiLSTM (without Physical Information Embedding)	6.0533	4.7124	2.7156%	0.99154
EEMD+TCN	5.1593	3.9434	2.0943%	0.99385
EEMD+BiLSTM	8.6904	7.1037	3.5017%	0.98256
TCN+BiLSTM	6.348	4.995	2.1535%	0.99069

Across all four forecasting scales, the dual-stream EEMD + TCN + BiLSTM consistently achieves the best error control and trend alignment, with the lowest RMSE and the smallest error growth rate as prediction length increases. Physical features enhance short-term sensitivity to acceleration events and constrain medium- and long-term evolution trends, enabling the dual-stream architecture to remain robust and reliable across multi-horizon extrapolation. In contrast, the remaining models exhibit increasing drift or oscillation as the forecasting horizon extends, indicating that the integration of multi-scale temporal features with physical dynamical information significantly improves cross-scale adaptability and robustness in landslide displacement prediction.

4 Multi-Scale Engineering Risk Indicators Based on Predicted Displacement

4.1 Short-Term Early Warning (Weekly Scale): Acceleration Sensitivity Index I_{acc}

Short-term early warning focuses on whether significant acceleration or pre-failure trends will occur within the next 1–7 days, which is directly related to organizing personnel evacuation and equipment relocation 24–48 hours in advance. Building upon the early-warning thresholds defined in the improved tangential-angle method [47] and the displacement rate–ratio method [48], this study develops a short-term Acceleration Sensitivity Index I_{acc}. Using the predicted displacement series, the daily mean velocity v_d is computed, and the velocity ratio $R_v = v_d/v_0$ is constructed with respect to the baseline steady-state velocity v_0 obtained during the historical quasi-linear stage. On the cumulative displacement–time curve, displacement increments and time intervals between adjacent observations form incremental vectors. The angle between these vectors and the time axis yields the improved tangential angle α_i, whose temporal evolution characterizes the transitions among creeping, steady

movement, and acceleration phases. By jointly considering the interval combinations of R_v and α_i, the short-term early-warning states are categorized into four levels:

Table 6. Classification of Short-term Early Warning Indicators.

Deformation Stage	Displacement Rate Ratio R_v	Improved Tangential Angle α_i	Warning Level	Warning Color
Constant-rate deformation	$0 \le R_v \le 2$	$\alpha_i \approx 45°$	Level I (Attention)	Blue Warning
Initial acceleration	$2 < R_v \le 6$	$45° < \alpha_i < 80°$	Level II (Alert)	Yellow Warning
Intermediate acceleration	$6 < R_v \le 8$	$80° \le \alpha_i < 85°$	Level III (Caution)	Orange Warning
Imminent failure	$R_v > 8$	$\alpha_i \ge 85°$	Level IV (Alarm)	Red Warning

Then put the left brackets I. subscript acc right brackets into the same discriminant table to realize the mapping from the model output to the short-term warning level (Fig.16).

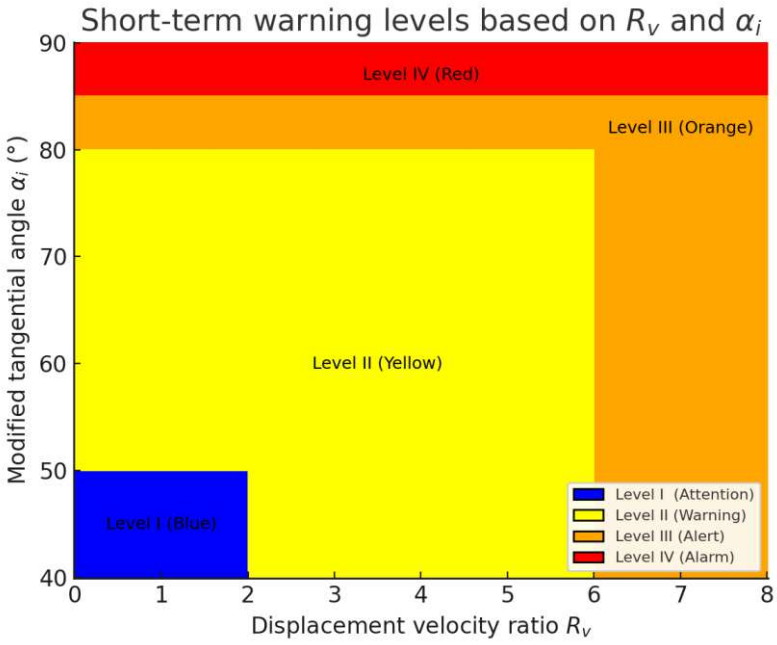


Fig. 16. Mapping of Risk Level Discrimination Indicators for Short-term Early Warning.

4.2 Medium-Term Early Warning (Monthly Scale): Trend Risk Index I_{trend}

Monthly-scale forecasting primarily supports engineering scheduling, pre-flood-season mitigation planning, and staged allocation of emergency funds. The key question is whether the landslide will exhibit a sustained deterioration trend in the coming month and whether it should be included in near-term stabilization plans. To address this need, a medium-term Trend Risk Index $I_{\text{trend}}$is developed based on the 30-day predicted displacement sequence, simultaneously accounting for both absolute deformation magnitude and relative amplification. First, the predicted displacement series $d(t)$for the next 30 days is differenced and averaged to obtain the monthly mean displacement rate $\bar{v}_{30}$(mm/d) and net settlement, which together reflect the overall deformation intensity. Meanwhile, using multi-year monitoring data, the mean background velocity $\bar{v}_{\text{bg}}$during characteristic steady-state periods is derived. The 30-day velocity ratio $R_{30} = \bar{v}_{30}/\bar{v}_{\text{bg}}$ is then computed to quantify the amplification of the predicted state relative to the long-term stable baseline.

To align with engineering practices, $\bar{v}_{30}$is annualized into an equivalent yearly rate ($v_{\text{yr}} \approx \bar{v}_{30} \times 365/30$) and compared with the velocity classification proposed by Cruden & Varnes [22], which identifies a critical threshold of approximately 1.6 m/yr (≈ 4.4 mm/d). This threshold is widely recognized as the boundary between a maintainable condition and an engineering-unacceptable state. Accordingly, this study adopts 4.5 mm/d as a key decision threshold for monthly risk classification. In addition, historical landslide data from Yunxi County, Shiyan—where clear acceleration or engineering interventions occurred—show daily displacement rates typically exceeding 6–10 mm/d. Based on this empirical upper range, 10 mm/d is used as the indicative threshold for entering the high-risk category. Supported by the

above theoretical basis and empirical observations, the four-level classification rules for I_{trend} are explicitly defined as follows:

Table 7. Classification of Medium-term Early Warning Indicators.

Mean Daily Rate $\bar{v}_{30}$	30-day Rate Ratio R_{30}	Warning Level	Warning Color	Engineering Intervention
$\bar{v}_{30} \leq 1.0$ mm/d	$0.5 \leq R_{30} < 1.5$°	Level I (Maintenance)	Blue Warning	Routine monitoring and field inspection
$1.0 < \bar{v}_{30} \leq 4.5$ mm/d	$1.5 \leq R_{30} < 3.0$	Level II (Attention)	Yellow Warning	Stability reassessment and preliminary reinforcement planning
$4.5 < \bar{v}_{30} \leq 10$ mm/d	$3.0 \leq R_{30} < 5.0$	Level III (Mitigation)	Orange Warning	Scheduling of specific drainage or reinforcement works
$\bar{v}_{30} > 10$ mm/d	$R_{30} \geq 5.0$	Level IV (Critical)	Red Warning	Inclusion in emergency mitigation projects

The monthly-scale trend risk index not only preserves the physical meaning of internationally accepted velocity classifications but also reflects the engineering sensitivity of this landslide site. It provides quantitative support for determining whether the landslide should be prioritized for stabilization within the next month.

4.3 Long-Term Forecasting (Quarterly Scale): Integrated Deformation Index I_{season}

Quarterly-scale forecasting primarily supports medium- to long-term engineering management tasks, including seasonal risk zoning, resource allocation during the flood season, budgeting for regional mitigation projects, and identification of cross-seasonal risk evolution.

These tasks require an integrated assessment over an extended temporal window, considering cumulative deformation, average displacement rate, and the frequency of acceleration events—factors that collectively indicate whether the landslide is approaching a structurally unstable state. Accordingly, this study constructs a long-term Integrated Deformation Index I_{season}, drawing inspiration from the Comprehensive Standard Deformation Index (CSDI) approach [52], and classifies it into four engineering-practical risk levels. From the 90-day predicted displacement sequence, three key indicators are extracted: maximum cumulative displacement $S_{\max}$, average displacement rate $\bar{v}_{90}$, and the number of significant acceleration days N_{acc}. These indicators respectively characterize the overall deformation magnitude, reflect long-term kinematic evolution, and capture seasonal abnormal behaviors. Each indicator is normalized using its historical extrema or mean values. Based on long-term monitoring data, empirical probability distributions for each indicator are estimated, and the cumulative probability for each predicted value is computed:

$$P_S = \text{CDF}(S_{\max}), P_v = \text{CDF}(\bar{v}_{90}), P_N = \text{CDF}(N_{\text{acc}}).$$

The integrated deformation index is then constructed using a weighted combination:

$$I_{\text{season}} = w_S P_S + w_v P_v + w_N P_N,$$

where the weights $(w_S, w_v, w_N)$are assigned based on the relative importance of structural deformation, deformation rate, and triggering factors as described in the *Code for Investigation of Landslide Prevention Engineering* [44], along with expert judgment from the study area (values: $w_S = 0.4,\ w_v = 0.35,\ w_N = 0.25$). Following CSDI-based methodologies and early-warning classification practices, the integrated index is divided into four intervals corresponding to extremely low, low, moderate, and high seasonal risk (Table 8, Fig. 17). This

enables a direct mapping from the predicted displacement results to regional risk zoning and seasonal funding allocation strategies.

Table 8. Classification of Long-term Early Warning Indicators.

Maximum Cumulative Displacement (S_{max})	Mean Rate ($\bar{v}_{90}$)	Days with Significant Acceleration (N_{acc})	Composite Index (I_{season})	Warning Level	Engineering Intervention
$S_{max} \leq S_{10\%}$ (within the lowest 10% of historical long-term deformation)	$\bar{v}_{30} \leq 1.0$ mm/d	$N_{acc} \leq 1$	$0.5 \leq R_{30} < 1.5$	Level I (Very Low Risk)	Routine inspection and monitoring
$S_{10\%} < S_{max} \leq S_{40\%}$	$1.0 < \bar{v}_{90} \leq 4.5$ mm/d	$1 < N_{acc} \leq 3$	$1.5 \leq R_{30} < 3.0$	Level II (Low Risk)	Pre-flood safety checks and drainage maintenance
$S_{40\%} < S_{max} \leq S_{70\%}$	$4.5 < \bar{v}_{90} \leq 10$ mm/d	$3 < N_{acc} \leq 6$	$3.0 \leq R_{30} < 5.0$	Level III (Moderate Risk)	Priority implementation in quarterly mitigation plans (e.g., drainage-trench repair, partial unloading, localized support or consolidation works)
$S_{max} > S_{70\%}$	$\bar{v}_{90} > 10$ mm/d	$N_{acc} > 6$	$R_{30} \geq 5.0$	Level IV (High Risk)	Key target for seasonal and pre-flood mitigation (annual reinforcement planning, budget allocation, short-

term stabilization, and full-cycle early-warning actions)

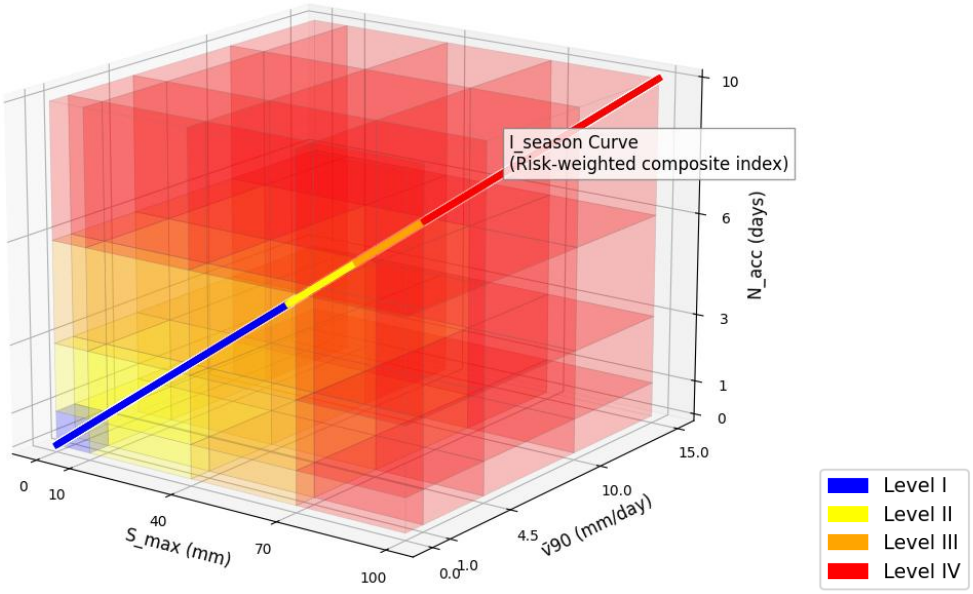


Fig. 17. Mapping of Risk Level Discrimination Indicators for Long-term Early Warning.

5 Digital-Twin-Driven Multi-Scale Engineering Scheduling and Decision-Making System for Landslides

Building upon the multi-scale prediction model and risk-indicator system established in the previous sections, this chapter further proposes embedding the entire workflow into a Digital Twin (DT) platform. Through a closed-loop mechanism, the DT system enables real-time monitoring, predictive analysis, risk classification, early-warning issuance, and engineering scheduling for landslide management. The system integrates physical consistency, data continuity, intelligent simulation, and engineering operability, thereby meeting the combined requirements of short-term early-warning response, medium-term mitigation planning, and long-term seasonal risk governance.

5.1 System Architecture of the Digital Twin for Landslide Risk Decision-Making

Considering the nonlinear, staged, and strongly coupled spatiotemporal characteristics of

landslide deformation, the proposed Digital Twin system consists of four layers: the state-perception layer, prediction–simulation layer, risk-interpretation layer, and engineering-scheduling layer, forming a full-cycle supervisory framework as shown in Fig. 18.

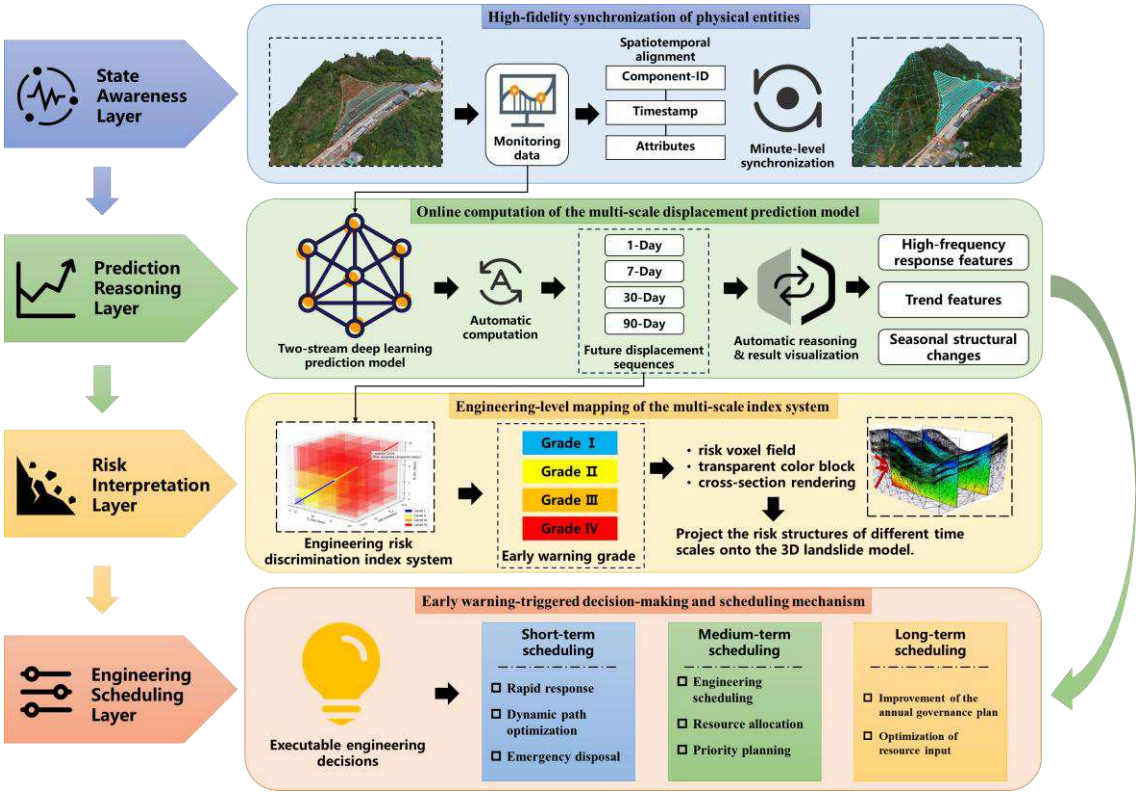


Fig.18. Hierarchical structure diagram of digital twin in landslide risk decision-making

(1) State-Perception Layer: High-Fidelity Synchronization of the Physical Entity

The system achieves minute-level synchronization of monitoring data using a unified data structure of "Spatial Entity (Component-ID) — Timestamp — Attributes" for spatiotemporal alignment. The digital twin maintains dynamic consistency with the physical landslide body, providing continuous and complete temporal inputs for downstream predictive models.

(2) Prediction–Simulation Layer: Online Multi-Scale Displacement Forecasting

The DT embeds the dual-stream deep learning model developed in Chapter 3. After each state update, the system automatically computes displacement predictions for 1-day, 7-day, 30-day, and 90-day horizons. Model inference is triggered automatically as new data arrive, and multi-

scale forecasts are visualized within the twin environment. High-frequency response characteristics, trend evolution, and seasonal structural variations from model outputs are mapped to corresponding elements of the DT's spatial representation.

(3) Risk-Interpretation Layer: Engineering-Oriented Mapping of Multi-Scale Indicators

Using the threshold system developed in Chapter 4, the DT automatically assigns four-level early-warning states. Risk fields are rendered through voxelization, semi-transparent overlays, and cross-sectional visualization, projecting multi-scale risk structures onto the 3D landslide body. This enables identification of spatial clusters of short-term acceleration, visualization of deformation-intensified regions at the monthly scale, and delineation of structurally controlled high-risk zones on the seasonal scale.

(4) Engineering-Scheduling Layer: Decision-Making Mechanisms Triggered by Early Warning

The engineering-scheduling layer transforms prediction and risk-interpretation outputs into actionable decisions. Short-term scheduling relies on high-frequency monitoring and a rule-based engine to support rapid response, dynamic path optimization, and emergency operations. Medium-term scheduling leverages simulation-based optimization for engineering task scheduling, resource allocation, and priority planning. Long-term scheduling draws upon the risk database, strategic planning tools, and cross-departmental coordination models to optimize annual mitigation programs and resource investment.

5.2 Application of the Digital Twin System to an Actual Engineering Landslide

To validate the practical value of the proposed digital-twin-based multi-scale engineering scheduling system, a representative landslide in Yunxi County, Shiyan City, Hubei Province was

selected for retrospective verification. The evaluation period spans from 1 July to 30 December 2024, covering the high-risk flood season. Through the state-perception layer, the system synchronizes GNSS displacement, tilt measurements, rainfall data, and other monitoring variables at a minute-level resolution, forming a complete digital twin of the physical landslide body (Fig. 19). This ensures continuous and coherent time-series inputs for the prediction and risk-interpretation modules.



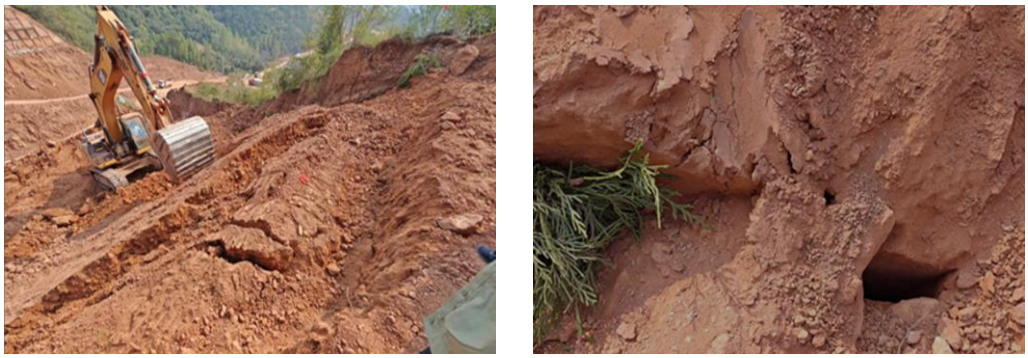
Fig. 19. Schematic Diagram of Landslide Digital Twin Visualization Early Warning and Decision-making Platform.

In the short-term forecast, the system issued a red early warning on July 12, 2024, for acceleration at the landslide toe triggered by rainfall. The digital twin immediately activated the emergency response mechanism (Fig. 20), automatically generating an optimized patrol route and dispatching seven inspectors to prioritize checks at the toe and other critical monitoring points. Personnel in hazardous zones were evacuated in time, and temporary drainage and support measures were rapidly deployed. Although a localized collapse occurred at the toe on the evening of July 14, the early warning provided by the digital twin enabled

687 successful avoidance of risk for both personnel and equipment, preventing casualties and
688 damage to key facilities.



(a) (b)

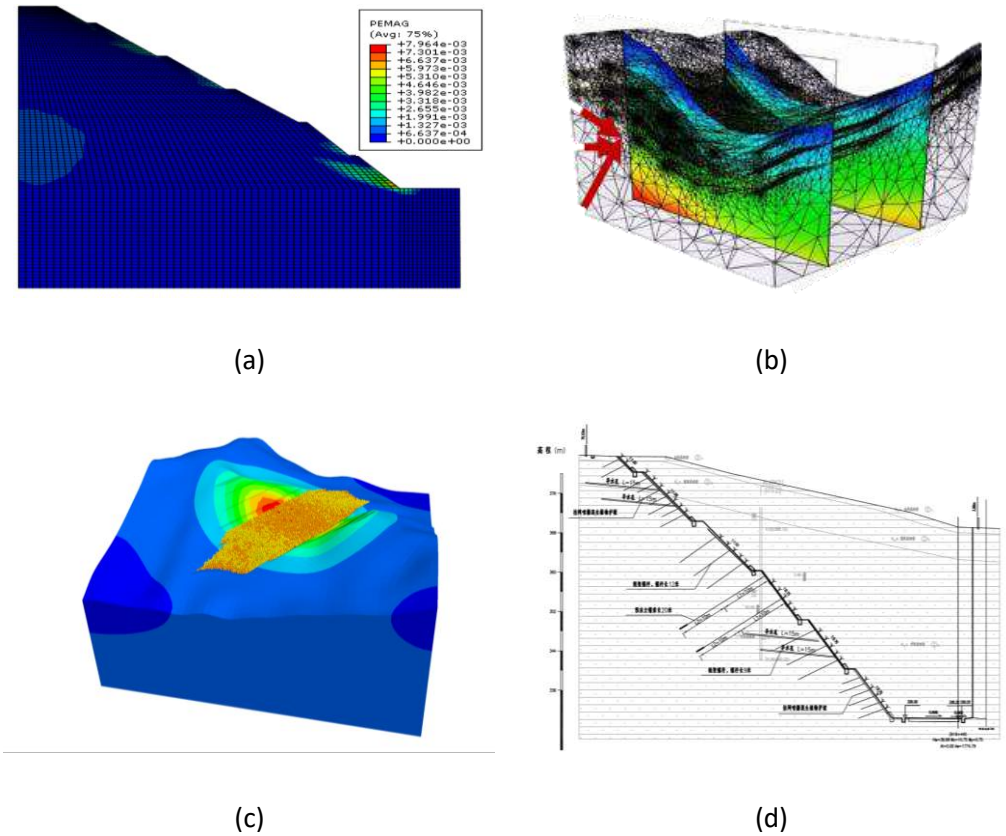


(c) （d）

689 **Fig. 20. Schematic Diagram of Landslide Short-term Early Warning: (a) Before Landslide**
690 **Collapse, (b) System Short-term Early Warning, (c) Landslide Sliding, (d) Slope Toe Cracks.**

691 In the medium-term forecast, starting from July 1, the system consistently identified significant
692 monthly-scale deformation trends at the mid-slope and western flank, issuing an orange
693 warning. Simulation results highlighted two creep bands with pronounced incremental
694 deformation. Based on simulation-driven optimization of construction risk and scheduling, the
695 digital twin generated a construction plan for drainage ditches, unloading trenches, and
696 support beams, specifying an optimized sequence of operations and resource allocation (Fig.
697 21). After implementation, the reinforcement of critical slope sections was completed as

planned, effectively controlling cumulative deformation of the landslide mass.



(a) (b)

(c) (d)

Fig. 21. Schematic Diagram of Landslide Medium-term Early Warning: (a) Digital Twin Simulation and Analysis, (b) Identification of Two Creep Zones, (c) Simulation-Optimized Construction Risks and Progress ,(d) Construction Scheduling Design of Drainage Ditches, Unloading Ditches and Support Beams

In the long-term forecast, the system integrated rainfall and predicted displacement to conduct seasonal risk assessments over the entire landslide. It predicted high-risk conditions during the flood season. Using the risk database and multi-department coordination, the digital twin produced an annual mitigation plan, including key pre-flood reinforcement, drainage, and monitoring arrangements, along with optimized funding and personnel deployment. The actual implementation followed the planned schedule, and the seasonal evolution of the landslide closely matched the predicted trends and risk assessments.

6 Discussion

The temporal–physical dual-stream model and the multi-scale landslide prediction and intelligent risk–decision framework developed in this study enable integrated management across short-term, monthly, and seasonal timescales. By directly mapping displacement forecasts to engineering actions, the system achieves a closed-loop workflow—from short-term emergency response to medium- and long-term mitigation planning. The results demonstrate that, for rainfall-induced landslides, the framework effectively identifies acceleration phases, optimizes resource allocation, and supports mitigation strategy formulation, confirming the engineering value of the dual-stream deep learning architecture. Nevertheless, several limitations remain. First, the current physical features primarily rely on derived kinematic indicators and do not fully incorporate multi-source information such as groundwater level, pore-water pressure, or subsurface geological structure, which may restrict predictive accuracy for complex or compound landslides. Second, the robustness and transferability of the model and indicators depend on the availability of high-quality monitoring data; missing or anomalous data may reduce decision reliability. Third, the adaptability of the system to extreme weather events or multi-trigger scenarios requires further evaluation. Overall, despite these limitations, the proposed approach offers a practical and deployable framework for intelligent, multi-scale landslide risk management and provides a reference pathway for future system enhancement and multi-source data integration.

7 Conclusions

This study develops a multi-timescale, full-lifecycle landslide forecasting and intelligent risk-decision framework that enables a complete closed loop from displacement prediction to

engineering scheduling. By combining EEMD-based signal decomposition with a dual-stream deep learning architecture that incorporates both temporal features (TCN–BiLSTM) and physically informed descriptors, the proposed model delivers accurate displacement predictions at daily, monthly, and seasonal timescales. Building on the forecasted displacement, three engineering-oriented risk indices were established: a short-term acceleration-sensitivity index, a medium-term trend-risk index, and a long-term integrated deformation index. These indicators translate model outputs into four actionable warning levels, supporting rapid emergency response, monthly construction planning, and quarterly mitigation strategies. The case study demonstrates that the dual-stream model reliably identifies rainfall-induced acceleration phases, maintains stable trend prediction over medium and long horizons, and significantly enhances robustness under nonstationary deformation conditions. The derived indices capture both transient and structural deformation characteristics, enabling quantitative and interpretable risk classification. Integrated within a digital twin environment, the system provides real-time visualization, multi-scale forecasting, and automated engineering decision support, forming a coherent workflow for landslide hazard management. Overall, this research establishes a comprehensive and operational technical chain that links predictive modeling, risk interpretation, and engineering scheduling. The proposed framework offers a scalable and transferable solution for intelligent landslide early warning and multi-timescale disaster mitigation, and provides a foundation for future developments that incorporate additional multi-source data and more advanced physical constraints.

Data Availability Statement

Some or all data, models, or code generated or used during the study are proprietary or confidential in nature and may only be provided with restrictions.

Funding

This research was supported by the project “Key Technologies for Intelligent and Green Construction of Highway Engineering in the Water Source Area of the South-to-North Water Diversion Project” (Grant No. CSCI-2024-Z-13).

Conflict of Interest

The authors declare that they have no known competing financial interests or personal relationships that could have appeared to influence the work reported in this paper.

REFERENCES:

[1] W. Gong, S. Zhang, C.H. Juang, H. Tang, S.P. Pudasaini, Displacement prediction of landslides at slope-scale: review of physics-based and data-driven approaches, Earth Sci. Rev. 258 (2024) 104948. https://doi.org/10.1016/j.earscirev.2024.104948.

[2] F.F. Mojtahedi, N. Yousefpour, S.H. Chow, M. Cassidy, Deep learning for time series forecasting: review and applications in geotechnics and geosciences, Arch. Comput. Methods Eng. 32 (2025) 3415–3445. https://doi.org/10.1007/s11831-025-10244-5.

[3] M. Yu, Q. Huang, Z. Li, Deep learning for spatiotemporal forecasting in Earth system science: a review, Int. J. Digital Earth. 17 (2024). https://doi.org/10.1080/17538947.2024.2391952.

[4] Y. Zhang, J. Tang, Y. Cheng, L. Huang, F. Guo, X. Yin, N. Li, Prediction of landslide displacement with dynamic features using intelligent approaches, Int. J. Min. Sci. Technol.

776 32 (2022) 539–549. https://doi.org/10.1016/j.ijmst.2022.02.004.
777 [5] H. Wang, P. Shao, H. Wang, F. Gan, C. Li, Y. Cen, X. Xu, A VMD-DES-TSAM-LSTM-based
778 interpretability multi-step prediction approach for landslide displacement, Environ. Earth
779 Sci. 83 (2024). https://doi.org/10.1007/s12665-024-11503-7.
780 [6] Z. Lin, Y. Ji, X. Sun, Landslide displacement prediction based on CEEMDAN method and
781 CNN–BiLSTM model, Sustainability. 15 (2023) 10071.
782 https://doi.org/10.3390/su151310071.
783 [7] J. Zhang, C. Lin, H. Tang, T. Wen, D.D. Tannant, B. Zhang, Input-parameter optimization
784 using a SVR based ensemble model to predict landslide displacements in a reservoir area
785 – a comparative study, Appl. Soft Comput. 150 (2024) 111107.
786 https://doi.org/10.1016/j.asoc.2023.111107.
787 [8] R. He, W. Zhang, J. Dou, N. Jiang, H. Xiao, J. Zhou, Application of artificial intelligence in
788 three aspects of landslide risk assessment: a comprehensive review, Rock Mech. Bull. 3
789 (2024). https://doi.org/10.1016/j.rockmb.2024.100144.
790 [9] Y. Wang, H. Tang, J. Huang, T. Wen, J. Ma, J. Zhang, A comparative study of different
791 machine learning methods for reservoir landslide displacement prediction, Eng. Geol. 298
792 (2022) 106544. https://doi.org/10.1016/j.enggeo.2022.106544.
793 [10] A. Dahal, L. Lombardo, Towards physics-informed neural networks for landslide prediction,
794 Eng. Geol. 344 (2025) 107852. https://doi.org/10.1016/j.enggeo.2024.107852.
795 [11] B. Yuan, C.S. Choo, L.Y. Yeo, Y. Wang, Z. Yang, Q. Guan, S. Suryasentana, J. Choo, H. Shen,
796 M. Megia, J. Zhang, Z. Liu, Y. Song, H. Wang, X. Chen, Physics-informed machine learning
797 in geotechnical engineering: a direction paper, Geomech. Geoeng. 20 (2025) 1128–1159.

https://doi.org/10.1080/17486025.2025.2502029.

[12] L. Wang, H. Zhang, X. Zhang, G. Peng, Z. Li, X. Xu, Deep temporal convolutional networks for F10.7 radiation flux short-term forecasting, Ann. Geophys. 42 (2024) 91–101. https://doi.org/10.5194/angeo-42-91-2024.

[13] J. Xu, Y. Jiang, C. Yang, Landslide displacement prediction during the sliding process using XGBoost, SVR and RNNs, Appl. Sci. 12 (2022) 6056. https://doi.org/10.3390/app12126056.

[14] H. Wen, B. Liu, M. Di, J. Li, X. Zhou, A SHAP-enhanced XGBoost model for interpretable prediction of coseismic landslides, Adv. Space Res. 74 (2024) 3826–3854. https://doi.org/10.1016/j.asr.2024.07.013.

[15] J. Li, X. Zhang, Ma Tao, P. Zeng, X. Yin, B. Han, P. Zhou, An interpretable landslide displacement prediction model based on xgboost and shap, J. Eng. Geol. 33 (2025) 1428–1438. https://doi.org/10.13544/j.cnki.jeg.2022-0856.

[16] G. Ren, L. Diao, F. Guo, T. Hong, A co-attention based multi-modal fusion network for review helpfulness prediction, Inf. Process. Manage. 61 (2024) 103573. https://doi.org/10.1016/j.ipm.2023.103573.

[17] Y. Jiang, K. Ning, Z. Pan, X. Shen, J. Ni, W. Yu, A. Schneider, H. Chen, Y. Nevmyvaka, D. Song, Multi-modal time series analysis: a tutorial and survey, in: Proceedings of the 31st ACM SIGKDD Conference on Knowledge Discovery and Data Mining V.2, Association for Computing Machinery, New York, NY, USA, 2025: pp. 6043–6053. https://doi.org/10.1145/3711896.3736567.

[18] D. Cruden, A simple definition of a landslide, Bull. Eng. Geol. Environ. 43 (1991) 27. https://doi.org/10.1007/BF02590167.

[19] M. Saito, Forecasting time of slope failure by tertiary creep, in: 1969: pp. 677–683.

[20] T. Fukuzono, A new method for predicting the failure time of slope, in: 1985: pp. 145–150.

[21] E. Hoek, J. Bray, Rock slope engineering. Revised second edition, in: International Journal of Rock Mechanics and Mining Sciences & Geomechanics Abstracts, 1977: p. A92. https://doi.org/10.1016/0148-9062(77)90892-0.

[22] D. Cruden, D.J. Varnes, Landslide types and processes, In: Turn. A.K. Schuster R.L. (Eds,) Landslides: Investig. Mitig., Natl. Acad. Press. D.C. 247 (1996) 36–75.

[23] F. Xie, L. Zhu, L. Wang, Modified grey system forecasting model and its application for analyzing information of landslide monitory, Yanshilixue Yu Gongcheng Xuebao/Chin. J. Rock Mech. Eng. 24 (2005) 4099–4105. https://doi.org/10.3321/j.issn:1000-6915.2005.22.015.

[24] H. Dong, H. Fu, W. Leng, W. Long, Boosting Ensemble of Support Vector Regression for Landslide Prediction, J. Hunan Univ.(Nat. Sci.). (2007) 6–10.

[25] Y. Yin, F. Wang, P. Sun, Landslide hazards triggered by the 2008 wenchuan earthquake, sichuan, china, Landslides. 6 (2009) 139–152. https://doi.org/10.1007/s10346-009-0148-5.

[26] B. Pradhan, A comparative study on the predictive ability of the decision tree, support vector machine and neuro-fuzzy models in landslide susceptibility mapping using GIS, Comput. Geosci. 51 (2013) 350–365. https://doi.org/10.1016/j.cageo.2012.08.023.

[27] B.T. Pham, D. Tien Bui, M.B. Dholakia, I. Prakash, H.V. Pham, A comparative study of least square support vector machines and multiclass alternating decision trees for spatial prediction of rainfall-induced landslides in a tropical cyclones area, Geotech. Geol. Eng. 34

(2016) 1807–1824. https://doi.org/10.1007/s10706-016-9990-0.

[28] Z. Liu, D. Guo, S. Lacasse, J. Li, B. Yang, J. Choi, Algorithms for intelligent prediction of landslide displacements, J. Zhejiang Univ.-Sci. A. 21 (2020) 412–429. https://doi.org/10.1631/jzus.A2000005.

[29] H. Jiang, Y. Li, C. Zhou, H. Hong, T. Glade, K. Yin, Landslide displacement prediction combining LSTM and SVR algorithms: a case study of shengjibao landslide from the three gorges reservoir area, Appl. Sci. 10 (2020) 7830. https://doi.org/10.3390/app10217830.

[30] M. Azarafza, M. Azarafza, H. Akgün, P.M. Atkinson, R. Derakhshani, Deep learning-based landslide susceptibility mapping, Sci. Rep. 11 (2021) 24112. https://doi.org/10.1038/s41598-021-03585-1.

[31] L. Nava, E. Carraro, C. Reyes-Carmona, S. Puliero, K. Bhuyan, A. Rosi, O. Monserrat, M. Floris, S.R. Meena, J.P. Galve, F. Catani, Landslide displacement forecasting using deep learning and monitoring data across selected sites, Landslides. 20 (2023) 2111–2129. https://doi.org/10.1007/s10346-023-02104-9.

[32] N.E. Huang, Z. Shen, S.R. Long, M.C. Wu, H.H. Shih, Q. Zheng, N.-C. Yen, C.C. Tung, H.H. Liu, The empirical mode decomposition and the hilbert spectrum for nonlinear and non-stationary time series analysis, Proc. R. Soc. Lond., A: Math. Phys. Eng. Sci. 454 (1998) 903–995. https://doi.org/10.1098/rspa.1998.0193.

[33] Z. Wu, N.E. Huang, Ensemble empirical mode decomposition: a noise-assisted data analysis method, Adv. Adapt. Data Anal. 1 (2009) 1–41. https://doi.org/10.1142/S1793536909000047.

[34] Z. Taorui, J. Hongwei, L. Qingli, Y. Kunlong, Landslide displacement prediction based on

variational mode decomposition and MIC-GWO-LSTM model, Stochastic Environ. Res. Risk Assess. 36 (2022) 1353–1372. https://doi.org/10.1007/s00477-021-02145-3.

[35] H. Wang, Y. Ao, C. Wang, Y. Zhang, X. Zhang, A dynamic prediction model of landslide displacement based on VMD–SSO–LSTM approach, Sci. Rep. 14 (2024) 9203. https://doi.org/10.1038/s41598-024-59517-2.

[36] C. Zhou, M. Ye, Z. Xia, W. Wang, C. Luo, J.-P. Muller, An interpretable attention-based deep learning method for landslide prediction based on multi-temporal InSAR time series: a case study of xinpu landslide in the TGRA, Remote Sens. Environ. 318 (2025) 114580. https://doi.org/10.1016/j.rse.2024.114580.

[37] G.E. Karniadakis, I.G. Kevrekidis, L. Lu, P. Perdikaris, S. Wang, L. Yang, Physics-informed machine learning, Nat. Rev. Phys. 3 (2021) 422–440. https://doi.org/10.1038/s42254-021-00314-5.

[38] M. Raissi, P. Perdikaris, G.E. Karniadakis, Physics-informed neural networks: a deep learning framework for solving forward and inverse problems involving nonlinear partial differential equations, J. Comput. Phys. 378 (2019) 686–707. https://doi.org/10.1016/j.jcp.2018.10.045.

[39] Z. Ma, G. Mei, Knowledge-infused deep learning enables interpretable landslide forecasting, (2023). https://doi.org/10.48550/arXiv.2307.08951.

[40] Y. Chen, Y. Wang, G. Huang, Q. Tian, Coupling physical factors for precipitation forecast in China with graph neural network, Geophys. Res. Lett. 51 (2024) e2023GL106676. https://doi.org/10.1029/2023GL106676.

[41] T. Carlà, P. Farina, E. Intrieri, H. Ketizmen, N. Casagli, Integration of ground-based radar

886 and satellite InSAR data for the analysis of an unexpected slope failure in an open-pit mine,
887 Eng. Geol. 235 (2018) 39–52. https://doi.org/10.1016/j.enggeo.2018.01.021.
888 [42] Y. Jin, X. Li, S. Zhu, B. Tong, F. Chen, R. Cui, J. Huang, Accurate landslide identification by
889 multisource data fusion analysis with improved feature extraction backbone network,
890 Geomatics Nat. Hazards Risk. 13 (2022) 2313–2332.
891 https://doi.org/10.1080/19475705.2022.2116357.
892 [43] X. Hu, Z. Sun, Z. Wang, X. Huang, M. Zhou, S. He, H. Xiao, D. Liu, Y. Yang, W. Xu, InSAR-
893 based deep learning prediction model for multi-type landslides displacement and failure
894 time in zigui, three gorges area, china, Landslides. (2025).
895 https://doi.org/10.1007/s10346-025-02613-9.
896 [44] Natural Resources and Territory Spatial Planning, GB/T 32864—2016 , Code for geological
897 investigation of landslide prevention, General Administration of Quality Supervision,
898 Inspection and Quarantine of the People / Standardization Administration of the People's
899 Republic of China, (2016).
900 https://openstd.samr.gov.cn/bzgk/gb/newGbInfo?hcno=9D81B87720C3992B619259738
901 446091E (accessed December 3, 2025).
902 [45] Department of International Cooperation and Science & Technology, Ministry of Natural
903 Resources of the People's Republic of China, DZ/T 0221—2006 , Monitoring code of
904 rockfall,landslide and debris flow, Standards Press of China, (2006).
905 https://std.samr.gov.cn/hb/search/stdHBDetailed?id=8B1827F26E4BBB19E05397BE0A0
906 AB44A (accessed December 3, 2025).
907 [46] Department of Natural Resources of Sichuan Province, DB51/T 3302-2025 , Technical

908 Specifications for the Combined Monitoring and Early Warning of Geological Hazards in
909 Sichuan Province, Administration for Market Regulation of Sichuan Province, (2025).
910 https://std.samr.gov.cn/db/search/stdDBDetailed?id=40DE903DAD131FFDE06397BE0A0
911 A57EC (accessed December 3, 2025).
912 [47] Q. Xu, Y. Zeng, J. Qian, C. Wang, C. He, Study on a improved tangential angle and the
913 corresponding landslide pre-warning criteria, Geol. Bull. China. 28 (2009) 501–505.
914 https://doi.org/10.3969/j.issn.1671-2552.2009.04.011.
915 [48] L. Wang, M. Xie, X. Chai, Research on method of displacement speed ratio for spatial
916 evaluation of landslide deformation, Rock Soil Mech. 35 (2014) 519–528.
917 https://doi.org/10.16285/j.rsm.2014.02.019.
918 [49] Y. Ben, W. Yi, X. Huang, Z. Wei, Y. Xiao, X. Deng, Progressive Warning Model for “Step-like”
919 Landslides Based on Effective Rainfall, South China Geol. 39 (2023) 492–501.
920 https://doi.org/10.3969/j.issn.2097-0013.2023.03.008.
921 [50] X. Huang, J. Xia, D. Lei, An early warning system for rainfall stepwise landslide based on
922 deformation monitoring, Chin. J. Geol. Hazard Control. 29 (2018) 68–76.
923 https://doi.org/10.16031/j.cnki.issn.1003-8035.2018.06.10.
924 [51] K. Georgieva, K. Smarsly, M. König, K.H. Law, An autonomous landslide monitoring system
925 based on wireless sensor networks, in: Computing in Civil Engineering (2012), American
926 Society of Civil Engineers, Clearwater Beach, Florida, United States, 2012: pp. 145–152.
927 https://doi.org/10.1061/9780784412343.0019.
928 [52] J. Zhang, H. Tang, B. Zhou, C. Li, Y. Zhang, Q. Tan, Landslide Early Warning Method, Device
929 and Storage Medium Based on Comprehensive Standard Deformation Index,

CN116612606A, 2023-8-18. https://kns.cnki.net/KCMS/detail/detail.aspx?dbcode=SCPD&dbname=SCPD202302&filename=CN116612606A (accessed December 3, 2025).

[53] L. Piciullo, M.T. Abraham, I.N. Drøsdal, E.S. Paulsen, An operational IoT-based slope stability forecast using a digital twin, Environ. Modell. Software. 183 (2025) 106228. https://doi.org/10.1016/j.envsoft.2024.106228.

[54] J. Xu, Y. Zhang, AI-powered digital twin technology for highway system slope stability risk monitoring, Geotechnics. 5 (2025). https://doi.org/10.3390/geotechnics5010019.

[55] X. Li, T. Chen, W. Xu, Z. Sun, L. Xue, X. Zhu, Z. Fan, H. Shan, Y. Jia, Research on Submarine Geohazard Monitoring and Early Warning Technology Based on Digital Twin, Period. Ocean Univ. China. 54 (2024) 102–114. https://doi.org/10.16441/j.cnki.hdxb.20230056.

[56] B. Tong, Y. Yin, B. Li, J. Tang, X. Yang, Z. Xu, Review on artificial intelligence-based large language models forgeological hazards, Chin. J. Geol. Hazard Control. 36 (2025) 1–12. https://doi.org/10.16031/j.cnki.issn.1003-8035.202503007.